

Modeling of Nanoscale Devices

M. P. Anantram¹, M. S. Lundstrom², and D. E. Nikonov³

¹ *Electrical and Computer Engineering Department,
University of Waterloo,
Ontario, Canada N2L 3G1*

² *Department of Electrical and Computer Engineering,
Purdue University, West Lafayette, IN 49097, USA and*

³ *Intel Corporation, Mail Stop: SC1-05
Santa Clara, CA 95052, USA*

I. INTRODUCTION

Semiconductor devices operate by controlling the flow of electrons and holes through a device, and our understanding of charge carrier transport has both benefited from and driven the development of semiconductor devices. When William Shockley wrote "Electrons and Holes in Semiconductors" [Sho50], semiconductor physics was at the frontier of research in condensed matter physics. Over the years, the essential concepts were clarified and simplified into the working knowledge of device engineers. The treatment of electrons and holes as semiclassical particles with an effective mass was usually adequate. Electronic devices were made of materials (e.g. silicon, gallium arsenide, etc.) with properties (e.g. bandgap, effective mass, etc.) that could be looked up. For most devices, the engineer's drift-diffusion equation provided a simple, but adequate description of carrier transport. Today things are changing. Device dimensions have shrunk to the nanoscale. The properties of materials can be engineered by intentional strain and size effects due to quantum confinement. Devices contain a countable number of dopants and are sensitive to structure at the atomistic scale. In addition to familiar devices like the MOSFET, which have been scaled to nanometer dimensions, new devices built from carbon nanotubes, semiconductor nanowires, and organic molecules are being explored. Device engineers will need to learn to think about devices differently. To describe carrier transport in nanoscale devices, engineers must learn how to think about charge carriers as quantum mechanical entities rather than as semiclassical particles, and they must learn how to think at the atomistic scale rather than at a continuum one. Our purpose in this chapter is to provide engineers with an introduction to the non-equilibrium Green's function (NEGF) approach, which provides a powerful conceptual tool and a practical analysis method to treat small electronic devices quantum mechanically and atomistically. We first review the basis for the traditional, semiclassical description of carriers that has served device engineers for more than 50 years in section II. We then describe why this traditional approach loses validity at the nanoscale. Next, we describe semiclassical ballistic transport in section III and the Landauer-Buttiker approach to phase coherent quantum transport in section IV. Realistic devices include interactions that break quantum mechanical phase and also cause energy relaxation. As a result, transport in nanodevices are between diffusive and phase coherent. We introduce the non equilibrium Green's function (NEGF) approach, which can be used to model devices all the way from ballistic to diffusive limits in section V. This is followed by a summary of equations that are used to model a large class of layered structures such as nanotransistors, carbon nanotubes and nanowires in section VI. An application of the NEGF method in the ballistic and scattering limits to silicon nanotransistors is discussed in sections VII and VIII respectively. We conclude with a summary in section IX. The Dyson's equations and algorithms to solve for the Green's functions of layered structures are presented in appendices B and C. These appendices can be left out by a reader whose aim is to gain a basic understanding of the NEGF approach to device modeling.

II. SEMICLASSICAL TRANSPORT: DIFFUSIVE

Electrical engineers have commonly treated electrons as semiclassical particles that move through a device under the influence of an electric field and random scattering potentials. As sketched in Fig. 1, electrons move along a trajectory in phase space (position and momentum space). In momentum space, the equation of motion looks like Newton's Law for a classical particle

$$\frac{d\hbar\vec{k}}{dt} = -\nabla_{\vec{r}}E_C(\vec{r}, t), \quad (1)$$

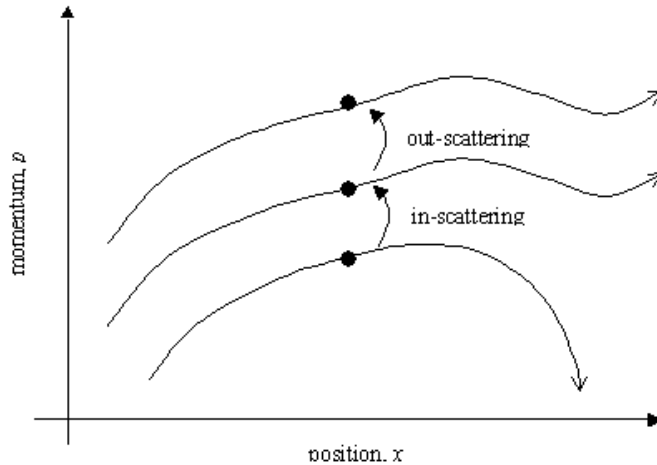


FIG. 1: Carrier trajectories in phase space showing free flights along a trajectory interrupted by scattering events that begin another free flight.

where \vec{k} is the crystal momentum and E_C is the bottom of the conduction band. In position space, the equation of motion is

$$\frac{d\vec{r}}{dt} = \frac{1}{\hbar} \nabla_{\vec{k}} E(\vec{k}), \quad (2)$$

where $E(k)$ describes the bandstructure of the semiconductor. The right hand side of eqn. (2) is simply the velocity of the semiclassical particle, and in the simplest case it is just $\hbar k/m^*$. By solving eqns. (1) and (2), we trace the trajectory of a carrier in phase space as shown in Fig. 1.

Equations (1) and (2) describe the ballistic transport of semiclassical carriers. In practice, carriers frequently scatter from various perturbing potentials (defects, ionized impurities, lattice vibrations, etc.). The result is that carriers hop from one trajectory in phase space to another as shown in Fig. 1. The average distance between scattering events, the mean-free-path, l , has (until recently) been much smaller than the critical dimensions of a device. Carriers undergo a random walk through a device with a small bias in one direction imposed by the electric field. To describe this scattering dominated (so-called diffusive) transport, we should add a random force ($F_S(\vec{r}, t)$) to the right hand side of eqn. (1)

$$\frac{d\hbar\vec{k}}{dt} = -\nabla_{\vec{r}} E_C(\vec{r}, t) + F_S(\vec{r}, t), \quad (3)$$

It is relatively easy to solve eqns. (1) and (3) numerically. One solves the equations of motion, eqns. (1) and (2) to move a particle through phase space. Random numbers are chosen to mimic the scattering process and occasionally kick a carrier to another trajectory. By averaging the results for a large number of simulated trajectories, these so-called Monte Carlo techniques provide a rigorous, though computationally demanding description of carrier transport in devices as described in [Jac89].

Device engineers are primarily interested in average quantities such as the average electron density, current density, etc. (There are some exceptions; noise is important too.) Instead of simulating a large number of particles, we can ask: What is the probability that a state at position, \vec{r} , with momentum $\hbar\vec{k}$, is occupied at time t ? The answer is given by the distribution function, $f(\vec{r}, \vec{k}, t)$, which can be computed by averaging the results of a large number of simulated trajectories. Alternatively, we can adopt a collective viewpoint instead of the individual particle viewpoint and formulate an equation for $f(\vec{r}, \vec{k}, t)$. The result is known as the Boltzmann Transport Equation (BTE),

$$\frac{\partial f}{\partial t} + \vec{v} \cdot \nabla_{\vec{r}} f - \frac{q\vec{E}}{\hbar k} \nabla_{\vec{k}} f = \hat{C}f \quad (4)$$

where \vec{E} is the electric field, and $\hat{C}f$ describes the effects of scattering. In equilibrium $f(\vec{r}, \vec{k}, t)$ is simply the Fermi function, but in general, we need to solve eqn. (4) to find f . Once $f(\vec{r}, \vec{k}, t)$ is known, quantities of interest to the device

engineer are readily found. For example, to find the average electron density in a volume Ω centered at position, \vec{r} , we simply add up the probability that all of the states in Ω are occupied and divide by the volume,

$$n(\vec{r}, t) = \frac{1}{\Omega} \sum_k f(\vec{r}, \vec{k}, t) . \quad (5)$$

Similarly, we find,

$$\text{Current Density} \quad \vec{J}(\vec{r}, t) = \frac{1}{\Omega} \sum_k (-q) \vec{v} f(\vec{r}, \vec{k}, t) , \quad (6)$$

$$\text{Kinetic Energy Density} \quad W(\vec{r}, t) = \frac{1}{\Omega} \sum_k E(\vec{k}) f(\vec{r}, \vec{k}, t) , \quad (7)$$

$$\text{Energy Current Density} \quad \vec{J}_E(\vec{r}, t) = \frac{1}{\Omega} \sum_k E(\vec{k}) \vec{v} f(\vec{r}, \vec{k}, t) , \quad (8)$$

where $q > 0$ is the absolute value of the electron charge. This approach provides a clear and fairly rigorous description of semiclassical carrier transport, but solving the six dimensional BTE is enormously difficult. One might ask if we can't just find a way to solve directly for the quantities of interest in eqns. (5) - (8). The answer is yes, but some simplifying assumptions are necessary.

Device engineers commonly describe carrier transport by few low order moments of the Boltzmann transport equation, eqn. (4). A mathematical prescription for generating moment equations exists, but to formulate them in a tractable manner, numerous simplifying assumptions are required [Lun00]. Moment equations provide a phenomenological description of transport that gives insight and quantitative results when properly calibrated.

The equation for the zeroth moment of $f(\vec{r}, \vec{k}, t)$ gives the well known continuity equation for the electron density, $n(\vec{r}, t)$,

$$\frac{\partial n(\vec{r}, t)}{\partial t} = -\nabla_r F_n + G_n - R_n , \quad (9)$$

where F_n is the electron flux,

$$J_n = -qF_n , \quad (10)$$

G_n the electron generation rate, and R_n the electron recombination rate. Equation (9) states that the electron density at a location increases with time if there is a net flux of electrons into the region (as described by the first term, minus the divergence of the electron flux) or if carriers are being generated there. Recombination causes the electron density to decrease with time. Any physical quantity must obey a conservation law like eqn. (9).

The equation for the first moment of $f(\vec{r}, \vec{k}, t)$ gives the equation for average current density (eqn. (6)) projection on the x -axis,

$$\frac{\partial J_{nx}}{\partial t} = \frac{2q}{m} \frac{dW_{xx}}{dx} + \frac{nq^2}{m^*} E_x - \frac{J_{nx}}{\tau_m} . \quad (11)$$

Each term on the right hand side of eqn. (11) is analogous to the corresponding terms in eqn. (9). The current typically changes slowly on the scale of the momentum relaxation time, τ_m , (typically a sub-picosecond time) so the time derivative can be ignored and eqn. (11) solved for

$$J_{nx} = nq\mu_n E_x + \frac{2}{3}\mu_n \frac{dW_{xx}}{dx} , \quad (12)$$

where

$$\mu_n = \frac{q\tau_m}{m^*} \quad (13)$$

is the electron mobility, and we have assumed equipartition of energy so that $W_{xx} = W/3$, where W is the total kinetic energy density. This assumption can be justified when there is a lot of isotropic scattering, which randomizes the carrier velocity. Eqn. (12) is a drift-diffusion equation; it says that electrons drift in electric fields and diffuse down kinetic energy gradients. Near equilibrium,

$$W = \frac{3}{2}nk_B T , \quad (14)$$

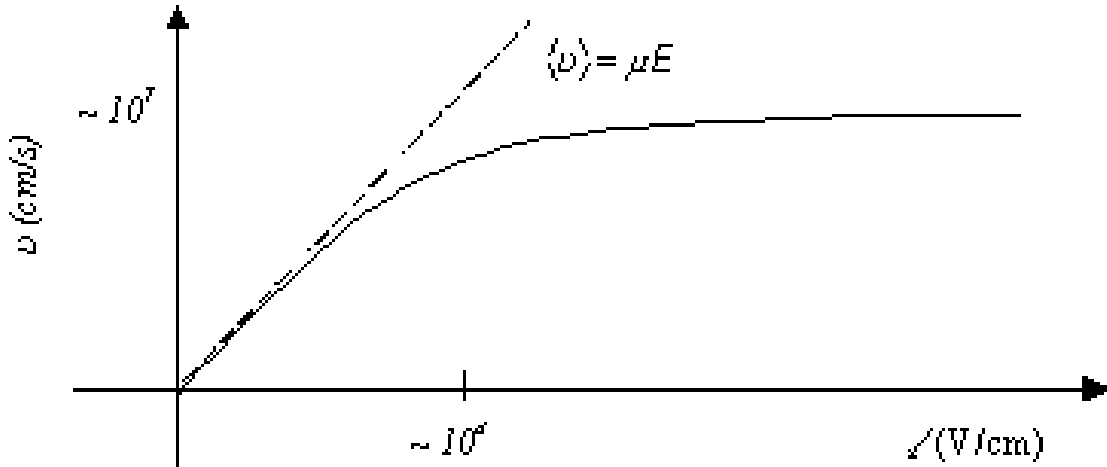


FIG. 2: The average velocity vs. electric field for electrons in bulk silicon at room temperature.

so when T is uniform, eqn. (12) becomes

$$J_{nx} = nq\mu_n E_x + k_B T \mu_n \frac{dn}{dx} = nq\mu_n E_x + qD_n \frac{dn}{dx}, \quad (15)$$

the drift-diffusion equation. By inserting eqn. (15) in the electron continuity equation, eqn. (9), we get an equation for the electron density that can be solved for the electron density within a device. This is the traditional and still most common approach for describing transport in semiconductor devices [Pie87].

Since most devices contain regions with high electric fields, the assumption that $W = 3nk_B T/2$ is not usually a good one. The carrier energy enters directly into the second term of the transport equation, eqn. (12), but it also enters indirectly because the mobility is energy dependent. To treat transport more rigorously, we need an equation for the electron energy.

The second moment of $f(\vec{r}, \vec{k}, t)$ gives the carrier energy density, $W(\vec{r}, t)$ according to eqn (8). The second moment of the BTE gives a continuity equation for the energy density [Lun00]

$$\frac{\partial W}{\partial t} = -\frac{dJ_W}{dx} + J_{nx} E_x - \frac{W - W_0}{\tau_E}, \quad (16)$$

where W_0 is the equilibrium energy density and τ_E the energy relaxation time. Note that the energy relaxation time is generally longer than the momentum relaxation time because phonon energies are small so that it takes several scattering events to thermalize an energetic carrier but only one to randomize its momentum.

To solve eqn. (16), we need to specify the energy current. The third moment of $f(\vec{r}, \vec{k}, t)$ gives the carrier energy flux, $J_W(\vec{r}, t)$ according to eqn. (8). The third moment of the BTE gives a continuity equation for the energy flux,

$$J_W = W\mu_E E_x + \frac{d(D_E W)}{dx}, \quad (17)$$

where μ_E and D_E are appropriate energy transport mobility and diffusion coefficient [Lun00].

Equations (9), (15), (16) and (17) can now be solved self-consistently to simulate carrier transport. Fig. (2) sketches the result for uniformly doped, bulk silicon with a constant electric field. At low electric fields, $W \sim 3nk_B T/2$, and we find that $\langle v_x \rangle \sim \mu_n E_x$. For electric fields above $\sim 10^4 V/cm$, the kinetic energy increases, which increases the rate of scattering and lowers the mobility so that at high fields the velocity saturates at $\sim 10^7 cm/s$. In a bulk semiconductor, there is a one-to-one relation between the magnitude of the electric field and the kinetic energy, so the mobility and diffusion coefficient can be parametrized as known functions of the local electric field. The result is that for bulk semiconductors or for large devices in which the electric field changes slowly, there is no need to solve all four equations; we need to solve the carrier continuity and drift-diffusion equations with field-dependent parameters.

Electric fields above $10^4 V/cm$ are common in nanoscale devices. This is certainly high enough to cause velocity saturation in the bulk, but in a short, high field region, transients occur. Fig. 3 illustrates what happens for a

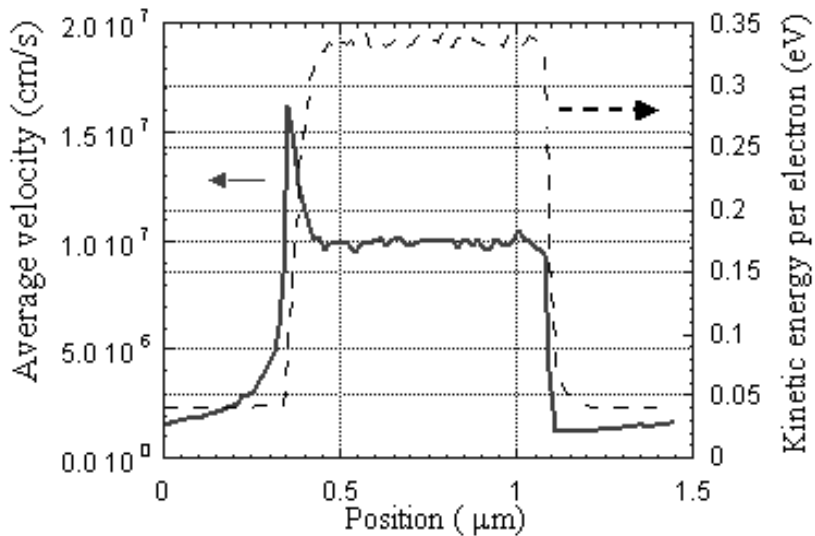


FIG. 3: The average steady-state velocity and kinetic energy vs. position for electrons injected into a short slab of silicon with low-high-low electric field profile.

hypothetical situation in which the electric field abruptly jumps from a low value to a high value and then back to a low value again. Electrons injected from the low field region are accelerated by the high electric field, but energy relaxation times are longer than momentum relaxation times, so the energy is slow to respond. The result is that the mobility is initially high (even though the electric field is high), so the velocity can be higher than the saturated value shown in Fig. 2. As the kinetic energy increases, however, scattering increases, the mobility drops, and the velocity eventually decreases to $\sim 10^7 \text{ cm/s}$, the saturated velocity for electrons in bulk silicon. The spatial width of the transient is roughly 100 nm; modern devices frequently have dimensions on this order, and strong velocity overshoot should be expected.

The example shown in Fig. 3 demonstrates that it is better to think of the mobility and diffusion coefficient as functions of the local kinetic energy rather than the local electric field. What this means is that eqns. (9), (15), (16) and (17) should all be solved self-consistently to simulate carrier transport in small devices. Device simulation programs commonly permit two options: 1) the solution of eqns. (9) and (15) self-consistently with the Poisson equation using mobilities and diffusion coefficients that depend on the local electric field (the so-called drift-diffusion approach) or 2) the solution of eqns. (9), (15), (16) and (17) self-consistently with the Poisson equation using mobilities and diffusion coefficients that depend on the local kinetic energy (so-called energy transport or hydrodynamic approaches). Solving the four equations self-consistently is more of a computational burden, but it is necessary for when the electric field changes rapidly on the scale of a mean-free-path for scattering. Actually, numerous simplifying assumptions are also necessary to even write the current and energy flux equations as eqns. (15) and (17) [Lun00]. The most rigorous (and computationally demanding) simulations (so-called Monte Carlo simulations) go back to the individual particle picture and track carriers trajectories according to eqns. (2) and (3). Drift-diffusion and energy transport approaches for treating carrier transport in semiconductor devices have two things in common; the first is the assumption that carriers can be treated as semiclassical particles and the second is the assumption that there is a lot of scattering. Both of these assumptions are losing validity as devices shrink.

III. SEMICLASSICAL TRANSPORT: BALLISTIC

Consider the "device" sketched in Fig. 4(a), which consists of a ballistic region attached to two contacts. The left contact (source) injects a thermal equilibrium flux of carriers into the device; some carriers reflect from the potential barriers within the device, and the rest transmit across and enter the right contact (drain). A similar statement

applies to the drain contact. The source and drain contacts are assumed to be perfect absorbers, which means that carriers impinging them from the device travel without reflecting back into the device. To compute the electron density, current, average velocity, etc. within the device, we have two choices. The first choice treats the carriers as semiclassical particles and the Boltzmann equation is solved to obtain the distribution function $f(\vec{r}, \vec{k}, t)$ as discussed in the previous section. The second choice treats the carriers quantum mechanically as discussed in the next section. In this section, we will use a semiclassical description in which the local density-of-states within the device is just that of a bulk semiconductor, but shifted up or down by the local electrostatic potential. This approximation works well when the electrostatic potential does not vary too rapidly, so that quantum effects can be ignored. To find how the k-states within the ballistic device are occupied, we solve the Boltzmann Transport Equation, eqn. (4). Because the device is ballistic, there is no scattering, and $\hat{C}f = 0$. It can be shown [Lun00] that the solution to the BTE with $\hat{C}f = 0$ is any function of the electron's total energy,

$$E = E_C(x) + E(k) \quad (18)$$

where, $E_C(x)$ is the conduction band minimum versus position and $E(k)$ is the band structure for the conduction band. We know that under equilibrium conditions sketched in Fig. 4(b), the proper function of total energy is the Fermi function,

$$f(E) = \frac{1}{1 + \exp\left(\frac{E - E_F}{k_B T}\right)}, \quad (19)$$

where the Fermi level, E_F , and temperature, T are constant in equilibrium.

Now consider the situation in Fig. 4c where a drain bias has been applied to the ballistic device. Although two thermal equilibrium fluxes are injected into the device, it is now very far from equilibrium. Since scattering is what drives the system to equilibrium, the ballistic device is as far from equilibrium as it can be. Nevertheless, for the ballistic device, the relevant steady-state Boltzmann equation is the same equation as in equilibrium. The solution is again a function of the carrier's total kinetic energy. At the contacts, we know that the solution is a Fermi function, which specifies the functional dependence on energy. For the ballistic device, therefore, the probability that a k-state is occupied is given by an equilibrium Fermi function. The only difficulty is that we have two Fermi levels, so we need to decide which one to use.

Return again to Fig. 4c and consider how to fill the states at $x = x_1$. We know that the probability that a k-state is occupied is given by a Fermi function, so we only need to decide which Fermi level to use for each k-state. For the positive k-states with energy above E_{TOP} , the top of the energy barrier, the states can only have been occupied by injection from the source, so the appropriate Fermi level to use is the source Fermi level. Similarly, negative k-states with energy above E_{TOP} can only be occupied by injection from the drain, so the appropriate Fermi level to use is the drain Fermi level. Finally, for k-states below E_{TOP} , both positive and negative velocity states are populated according to the drain Fermi level. The negative velocity k-states are populated directly by injection from the drain and the positive k-states are populated when negative velocity carriers reflect from the potential barrier.

Ballistic transport can be viewed as a special kind of equilibrium. Each k-state is in equilibrium with the contact from which it was populated. Using this reasoning, one can compute the distribution function and any moment of it (e.g. carrier density, carrier velocity, etc.) at any location within the device. Figure 5 shows that computed distribution function in a ballistic nanoscale MOSFET under high gate and drain bias [Rhe02]. A strong ballistic peak develops as carriers are injected from the source are accelerated in the high electric field near the drain. Each k-state is in equilibrium with one of the two contacts, but the overall carrier distribution is very different from the equilibrium Fermi-Dirac distribution. When scattering dominates, carriers quickly lose their "memory" of which contact they were injected from, but for ballistic transport there are two separate streams of carriers; one injected from the source and one from the drain.

To evaluate the electron density vs. position within the ballistic device, we should compute a sum like eqn. (5), but we must do two sums. one for the states filled from the left contact and another for the states filled from the right contact,

$$n(x) = \sum_{k_L} \Theta_L(x) f_L(E) + \sum_{k_R} \Theta_R(x) f_R(E), \quad (20)$$

where f_L and f_R are the equilibrium Fermi functions of contacts L and R and $\Theta_{L,R}(x)$ is a function that selects out the k-states at position, x, that can be filled by contact L or R according to the procedure summarized in Fig. 4. It is often convenient to do the integrals in energy space rather than in k-space in which case, eqn. (20) becomes

$$n(x) = \int dE \left[LDOS_L(x, E) f_L(E) + \int LDOS_R(x, E) f_R(E) \right] \quad (21)$$

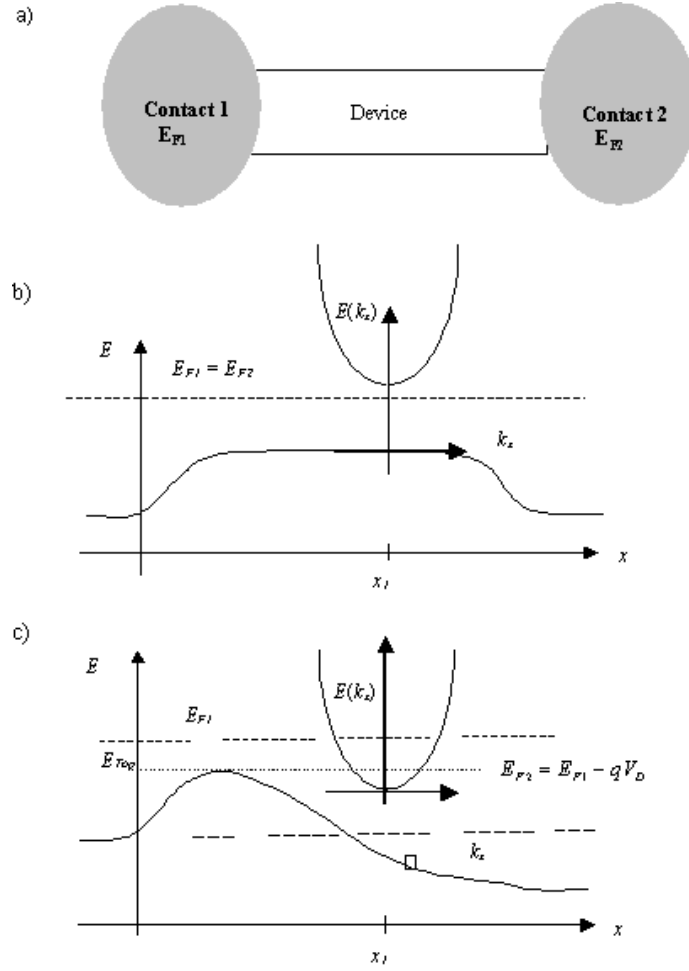


FIG. 4: Sketch of a ballistic device with two contacts that function as reservoirs of thermal equilibrium carriers. (a) Device and the two contacts. (b) Energy band diagram under equilibrium conditions ($V_D = 0$). (c) Energy band diagram under bias ($V_D > 0$).

where $LDOS_{L,R}(x, E)$ is the local density of states at energy E , fillable from contact L or R. For diffusive transport, we deal with a single density-of-states and fill it according to a single quasi-Fermi level, but for ballistic devices, the density of states separates into parts fillable from each contact.

The current flowing from source to drain (drain to source) contact is simply the transmission probability $T(E)$, times the Fermi function of the source (drain) contact. The net current flowing in the device is then,

$$I = \frac{e}{h} 2 \int dE T(E) [f_L(E) - f_R(E)] . \quad (22)$$

For the semiclassical example of Fig. 4, $T(E)=0$ for $E < E_{TOP}$ and $T(E)=1$ for $E > E_{TOP}$.

IV. PHASE COHERENT QUANTUM TRANSPORT: THE LANDAUER-BUTTIKER FORMALISM

Quantum mechanically the electron is a wave and the wave function $\Psi(\vec{r})$ is obtained by solving Schrodinger's equation,

$$\left[-\frac{\hbar^2}{2m} \nabla^2 + V(\vec{r}) \right] \Psi_n(\vec{r}) = E_n \Psi_n(\vec{r}) , \quad (23)$$

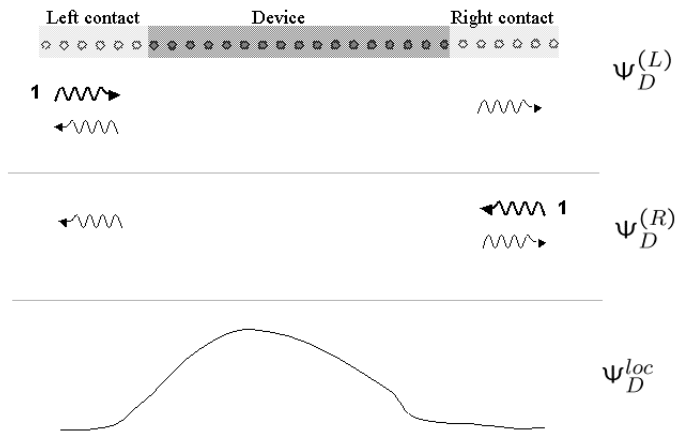


FIG. 5: All wave functions in the device can be represented as left incident ($\Psi_D^{(L)}$), right incident ($\Psi_D^{(R)}$) or localized states ($\Psi_D^{(loc)}$).

where E_n is the energy. Consider a device connected to two contacts as shown in Fig. 5, where the contacts are assumed to have a constant electrostatic potential. In a manner identical to the discussion of semiclassical modeling in the previous section, where we considered corpuscular electrons incident from the left and right contacts, in quantum mechanical modeling, we need to consider electron waves incident from the left and right contacts. The electron wave function in device region D can be thought to arise from:

- Waves incident from left lead of the form e^{ikx} , which have transmitted and reflected components $te^{ik'x}$ and re^{ikx} in the right and left leads respectively. The wave function in the device region D due to this wave is represented by $\Psi_D^{(L)}$.
- Waves incident from right lead of the form e^{-ikx} , which have transmitted and reflected components $te^{-ik'x}$ and re^{ikx} in the right and left leads respectively. The wave function in the device region D due to this wave is represented by $\Psi_D^{(R)}$.
- States localized in Device region represented by $\Psi_D^{(loc)}$. Localized and quasi-localized states are filled up by scattering due to electron-phonon and electron-electron interaction. We will assume here that localized states are absent.

The Landauer-Buttiker approach expresses the expectation value of an operator in terms of the left and right incident electrons from the contacts and their distribution functions. The expectation value of operator \hat{Q} is:

$$Q = \sum_{k,s} \left[\langle \Psi_D^{(L)} | \hat{Q} | \Psi_D^{(L)} \rangle f_L(E) + \langle \Psi_D^{(R)} | \hat{Q} | \Psi_D^{(R)} \rangle f_R(E) \right]. \quad (24)$$

Here the summation is performed over the momentum, k , and the spin, s , states. Since in this chapter we do not consider any spin-dependent phenomena, the spin summation translates into a factor of 2. We will distinguish this factor by keeping in front of sums and integrals. Eq. (24) has contributions from two physically different sources. The first term corresponds to contribution from waves incident from the left contact ($\Psi_D^{(L)}$) at energy E , weighted by the Fermi factor of the left contact (f_L). The second term corresponds to waves incident from the right contact ($\Psi_D^{(R)}$) weighted by the Fermi factor of the right contact (f_R). More generally, if region D is connected to a third contact G , then the expectation value of operator \hat{Q} is,

$$Q = \sum_{k,s} \left[\langle \Psi_D^{(L)} | \hat{Q} | \Psi_D^{(L)} \rangle f_L(E) + \langle \Psi_D^{(R)} | \hat{Q} | \Psi_D^{(R)} \rangle f_R(E) + \langle \Psi_D^{(G)} | \hat{Q} | \Psi_D^{(G)} \rangle f_G(E) \right], \quad (25)$$

where $\Psi_D^{(G)}$ corresponds to the wave function in the Device due to waves incident from contact G and f_G is the Fermi factor of contact G . Using eqn. (24), the contribution to electron (n) and current (J) densities at x in the device region D are given by,

$$n(x) = \sum_{k,s} \left[|\Psi_D^{(L)}(x)|^2 f_L(E) + |\Psi_D^{(R)}(x)|^2 f_R(E) \right] \quad (26)$$

and

$$J(x) = \sum_{k,s} \frac{e\hbar}{2mi} \left[\Psi_D^{(L)}(x) \dagger \frac{d\Psi_D^{(L)}(x)}{dx} f_L(E) + \Psi_D^{(R)}(x) \dagger \frac{d\Psi_D^{(R)}(x)}{dx} f_R(E) - c.c \right]. \quad (27)$$

The quantum mechanical density of states at energy E due to waves incident from the left ($LDOS_L$) and right ($LDOS_R$) are:

$$LDOS_L(x, E) = 2 \sum_{\text{k states with energy E incident from the left contact}} |\Psi_D^{(L)}(x)|^2 \quad (28)$$

$$LDOS_R(x, E) = 2 \sum_{\text{k states with energy E incident from the right contact}} |\Psi_D^{(R)}(x)|^2. \quad (29)$$

Then the electron density can be written in the same form as eqn. (21),

$$n(x) = \int LDOS_L(x, E) f_L(E) dE + \int LDOS_R(x, E) f_R(E) dE, \quad (30)$$

except that the expressions for the local density of states are different. Similarly, eqn. (27) can be expressed in a form identical to eqn. (22). The above formalism can be extended to calculate noise (shot and Johnson-Nyquist) in nanodevices [Buttiker92]. Device modeling in the phase coherent limit involves solving Schrodinger's equation to obtain the electron density self-consistently with Poisson's equation.

V. QUANTUM TRANSPORT WITH SCATTERING: THE NEED FOR GREEN'S FUNCTIONS

The description in the previous section is valid only in the phase coherent limit. The terminology "phase coherent" refers to a deterministic evolution of both the amplitude and phase of $\Psi_n(\vec{r})$ as given by Schrodinger's equation. The quantum mechanical wave function evolves phase coherently only in the presence of rigid scatterers, a common example of which is the electrostatic potential felt by an electron in the device. The wave function of an electron loses phase coherence due to scatterers which have an internal degree of freedom such as phonons. Phase incoherent scattering involves irreversible loss of phase information to phonon degrees of freedom. Naturally, including loss of phase information is important when device dimensions become comparable to the scattering lengths due to phonons and other phase breaking mechanisms. Accurate modeling of nanodevices should have the ability to capture:

- Interference effects
- Quantum mechanical tunneling
- Discrete energy levels due to confinement in 2D and 3D device geometries
- Scattering mechanisms (electron-phonon, electron-electron).

The first three effects can be modeled by solving Schrodinger's equation in a rigid potential as discussed in section IV. While in the semiclassical device modeling, the Boltzmann equation accounts for the energy and momentum relaxation due to scattering mechanisms, in quantum mechanical device modeling, the NEGF approach is necessary to account for energy, momentum and quantum mechanical phase relaxation.

In the remainder of this section, we explain the NEGF approach in the phase coherent limit by starting from Schrodinger's equation [Dat96]. We will start by an explanation of the tight binding Hamiltonian and relate this Hamiltonian to a device with open boundary conditions (section V A). The open boundary conditions lead to an infinite dimensional matrix. We will describe a procedure to fold the effect of the open boundaries into the finite device region in section V B. This will allow us to deal with small matrices where the open boundaries are modeled by *contact self energies*. The Green's functions, self energies and their relationship to current and electron density are derived in section V C. Then in section V D, we extend the discussion in section V C to one include electron-phonon interaction, which is where the NEGF approach is really essential.

B. Eliminating the Left and Right semi-infinite leads

A typical nanodevice can be conceptually divided into three regions (Fig. 6):

- Left semi-infinite lead (L) with a constant potential ϵ_l
- Device (D) with an arbitrary potential, and
- Right semi-infinite lead (R) with a constant potential ϵ_r .

The potential of the left (right) lead ϵ_l (ϵ_r) and the hopping parameter t_l (t_r) are assumed to be constant, which signifies that the leads are highly conducting and uniform. Then the Hamiltonian of the device and leads, eqn. (36), is an infinite dimensional matrix that can be expanded as,

$$\begin{aligned} & \bullet \\ & \bullet \\ & -t_l\Psi_{l-1} + (E - \epsilon_l)\Psi_{l0} - t_{l,d}\Psi_1 = 0 & (38) \\ & -t_{d,l}\Psi_{l0} + (E - \epsilon_1)\Psi_1 - t_{1,2}\Psi_2 = 0 & (39) \\ & -t_{1,2}\Psi_1 + (E - \epsilon_2)\Psi_2 - t_{2,3}\Psi_3 = 0 & (40) \\ & -t_{n-1,n}\Psi_{n-1} + (E - \epsilon_n)\Psi_n - t_{d,r}\Psi_{rn+1} = 0 & (41) \\ & -t_{r,d}\Psi_n + (E - \epsilon_r)\Psi_{rn+1} - t_r\Psi_{rn+2} = 0 & (42) \\ & \bullet \\ & \bullet \end{aligned}$$

where, the bullets represent the semi-infinite Left and Right leads. The subscript lm (rm) refer to grid point m in the Left (Right) lead. However, to find the electron density in eqn. (26), the wave function is only required at the device grid points. We will now discuss a procedure to fold the influence of the left and right semi-infinite leads into the device region.

Terminating the semi-infinite Left and Right leads: The wave function in the contacts due to waves incident from the left lead are,

$$\Psi_{ln} = (e^{+ik_l n} + s_{ll}e^{-ik_l n})u_{ln} \quad \text{in region L} \quad (43)$$

$$\Psi_{rn} = s_{rl}e^{ik_r n}u_{rn} \quad \text{in region R,} \quad (44)$$

and the corresponding eigen values are [eqn. (33)],

$$E - \epsilon_l = 2t_l \cos(k_l a) = t_l(e^{ik_l a} + e^{-ik_l a}), \quad (45)$$

and similarly for the right contact, with the indices r . s_{ll} and s_{rl} are the reflection and transmission amplitudes. Substituting Eqs. (43) and (45) in eqn. (38) yields,

$$s_{ll} = t_l^{-1}(-t_l + t_{ld}\Psi_1). \quad (46)$$

Substituting Eqs. (43) and (46) in eqn. (39), we obtain,

$$(E - \epsilon_1 - t_{d,l}e^{+ik_l a}t_l^{-1}t_{l,d})\Psi_1 + t_{1,2}\Psi_2 = -2it_{d,l}\sin(k_l a) \quad (47)$$

Eq. (47) is a modification of Schrodinger's equation centered at grid point 1 of the Device (eqn. (39)) to include the influence of the entire semi-infinite Left lead. Similarly, substituting eqn. (44) and $E - \epsilon_r = 2t_r \cos(k_r a)$ in eqn. (42) we get,

$$s_{rl} = t_r^{-1}t_{d,r}\Psi_n. \quad (48)$$

Now, substituting Eqs. (44) and (48) in eqn. (41), we can terminate the right semi infinite region to yield,

$$-t_{n-1,n}\Psi_{n-1} + (E - \epsilon_n - t_{d,r}e^{ik_r a}t_r^{-1}t_{r,d})\Psi_n = 0. \quad (49)$$

Eq. (49) is a modification of Schrodinger's equation centered at grid point n of the Device (eqn. (41)) to include the influence of the entire semi-infinite Right lead.

The influence of the semi-infinite Left and Right leads have been folded into grid points 1 and n of the device, for waves incident from the Left lead [Eqs. (47) and (49)]. Now the wave function in the device due to waves incident from the left lead can be obtained by solving the following n dimensional matrix instead of the infinite dimensional matrices in eqns. (38) - (42):

$$A\Psi_D^{(L)} = i_L, \quad (50)$$

where, A is a square matrix of dimension n , $\Psi_D^{(L)}$ and i_L are n by 1 vectors. i_L is the source function at (k, E) due to the Left lead. Matrix A is,

$$A = EI - H_D - \Sigma_{lead} \quad (51)$$

and the non zero elements of Σ_{lead} are,

$$\Sigma_{lead_{1,1}} = t_{d,l}e^{+ik_l a}t_l^{-1}t_{l,d} = \Sigma_L \quad (52)$$

$$\Sigma_{lead_{n,n}} = t_{d,r}e^{+ik_r a}t_r^{-1}t_{r,d} = \Sigma_R. \quad (53)$$

Σ_L and Σ_R are called the **self-energies**, and they represent the influence of the semi-infinite Left and Right leads on the Device respectively. The real part of self-energy shifts the on-site potential at grid point 1 from ϵ_1 to $\epsilon_1 + \text{Re}(\Sigma_L)$. The imaginary part of self energy multiplied by -2 is the scattering rate of electrons from grid point 1 of Device to Left lead (scattering rate = $-2\text{Im}[\Sigma_L]$), in the weak coupling limit.

In a manner identical to the derivation of eqn. (50), for waves incident from right contact, the wave function in the device ($\Psi_D^{(R)}$) can be obtained by solving:

$$A\Psi_D^{(R)} = i_R, \quad (54)$$

where i_R is the source function due to the Right semi infinite contact. The only non zero elements of A , i_L and i_R are:

$$A(1,1) = E - \epsilon_1 - \Sigma_L \text{ and } A(n,n) = E - \epsilon_n - \Sigma_R \quad (55)$$

$$A(i,i) = E - \epsilon_i, A(i,i+1) = -t_{i,i+1} \text{ and } A(i+1,i) = -t_{i,i+1}^\dagger \quad (56)$$

$$i_L(1) = -2it_{d,l}\sin(k_l a) \text{ and} \quad (57)$$

$$i_R(n) = -2it_{d,r}\sin(k_r a). \quad (58)$$

C. Electron and current densities expressed in terms of Green's functions

The Green's function corresponding to Schrodinger's equation ($[E - H]\Psi = 0$) for the device and contacts is,

$$[E - H + i\eta]G = I, \quad (59)$$

where η is an infinitesimally small positive number which pushes the poles of G to the lower half plane in complex energy, and H is the Hamiltonian. The Green's function of device region D with the influence of the contacts included is,

$$AG = I, \quad (60)$$

where

$$A = EI - H_D - \Sigma_{lead}(E) \quad (61)$$

is an n dimensional matrix defined in eqns. (55) and (56). The formal derivation of eqn. (60) is given in the appendix A.

Using the definition for G in Eqs. (50) and (54), the wave function in region D due to waves incident from Left and Right contacts can be written as,

$$\Psi_D^{(L)} = Gi_L \quad \text{and} \quad (62)$$

$$\Psi_D^{(R)} = Gi_R. \quad (63)$$

As i_L and i_R are non zero only at grid points 1 and n , the full G matrix is not necessary to find the wave function in the device; Only the two columns $G(:, 1)$ and $G(:, n)$ are necessary.

The **electron density** at grid point q can now be written using eqns. (62) and (63) in eqn. (26) as

$$n_q = \sum_{k,s} G_{q,1} i_L i_L^\dagger G_{1,q}^\dagger f_L + G_{q,n} i_R i_R^\dagger G_{n,q}^\dagger f_R \quad (64)$$

$$= \sum_{k,s} G_{q,1} [4t_{d,l} \sin^2(k_l a) t_{l,d} f_L] G_{1,q}^\dagger + G_{q,n} [4t_{d,r} \sin^2(k_r a) t_{r,d} f_R] G_{n,q}^\dagger, \quad (65)$$

where G^\dagger is the Hermitean conjugate of the Green's function. The summation over k can be converted to an integral over E by,

$$\sum_k \rightarrow \int \frac{dE}{2\pi} \left| \frac{dk}{dE} \right|. \quad (66)$$

Using eqn. (66) and $\left| \frac{dk}{dE} \right| = 2a|t| |\sin(k_l a)|$, eqn. (65) becomes,

$$n_q = 2 \int \frac{dE}{2\pi} \left[G_{q,1}(E) \Sigma_L^{in}(E) G_{1,q}^\dagger(E) + G_{q,n}(E) \Sigma_R^{in}(E) G_{n,q}^\dagger(E) \right] \cdot \frac{1}{a}, \quad (67)$$

where,

$$\Sigma_L^{in}(E) = 2t_{d,l} \frac{1}{|t|} |\sin(k_l a) t_{l,d} f_L(E) \quad \text{and} \quad (68)$$

$$\Sigma_R^{in}(E) = 2t_{d,r} \frac{1}{|t|} |\sin(k_r a) t_{r,d} f_R(E) . \quad (69)$$

k_l and k_r at energy E are determined by $E = \epsilon_l - 2t_l \cos(k_l a)$ and $E = \epsilon_r - 2t_r \cos(k_r a)$ (eqn. (33)) respectively. It can be seen from Eqs. (52), (53), (68) and (69):

$$\Sigma_L^{in}(E) = -2Im[\Sigma_L(E)] f_L(E) \quad (70)$$

$$\Sigma_R^{in}(E) = -2Im[\Sigma_R(E)] f_R(E) . \quad (71)$$

The electron density [eqn. (67)] can then be written as,

$$n_q = 2 \int \frac{dE}{2\pi} G(E) \Sigma_{lead}^{in}(E) G^\dagger(E) |_{q,q} \cdot \frac{1}{a}, \quad (72)$$

where, the non zero elements of Σ_{lead}^{in} are

$$\Sigma_{lead_{1,1}}^{in}(E) = \Sigma_L^{in}(E) \quad \text{and} \quad (73)$$

$$\Sigma_{lead_{n,n}}^{in}(E) = \Sigma_R^{in}(E). \quad (74)$$

Σ_L^{in} and Σ_R^{in} defined above in Eqs. (70) and (71) are called the **in-scattering self-energies** due to contacts. These self-energies physically represent in-scattering of electrons from the semi-infinite leads to the device and so play an important role in determining the charge occupancy in the device. They depend on the Fermi-Dirac factor / occupancy in the contacts f_L and f_R , and the strength of coupling between contacts and device, $Im[\Sigma_L(E)]$ and $Im[\Sigma_R(E)]$. It is easy to see using eqns. (72) and (74) that the electron density can also be written as,

$$n_q = \int dE [LDOS_L(q, E) f_L(E) + LDOS_R(q, E) f_R(E)], \quad (75)$$

where, $LDOS_L(q, E)$ ($LDOS_R(q, E)$) are the density of states due to waves incident from the left (right) contact, at grid point q , and

$$LDOS_L(q, E) = \frac{G_{q,1} \Gamma_L G_{1,q}^\dagger}{\pi} \cdot \frac{1}{a} \quad (76)$$

$$LDOS_R(q, E) = \frac{G_{q,n} \Gamma_R G_{n,q}^\dagger}{\pi} \cdot \frac{1}{a}, \quad (77)$$

where,

$$\Gamma_L(E) = -2Im[\Sigma_L(E)] \quad (78)$$

$$\Gamma_R(E) = -2Im[\Sigma_R(E)]. \quad (79)$$

Note that eqn. (75) is identical to eqn. (21) for semiclassical ballistic transport.

The **current density** between grid points q and $q+1$ per unit energy can be written as [eqn. (27)],

$$J_{q \rightarrow q+1}(E) = \frac{e\hbar}{2mai} 2[(\Psi_q^{(L)\dagger} \Psi_{q+1}^{(L)} - \Psi_{q+1}^{(L)\dagger} \Psi_q^{(L)}) f_L(E) + (\Psi_q^{(R)\dagger} \Psi_{q+1}^{(R)} - \Psi_{q+1}^{(R)\dagger} \Psi_q^{(R)}) f_R(E)]. \quad (80)$$

Now, following the derivation for electron density above [eqn. 67], it is straight forward to derive that the current density

$$J_{q \rightarrow q+1} = \frac{ie\hbar}{2ma^2} 2 \int \frac{dE}{2\pi} [G_{q,1}(E) \Sigma_L^{in}(E) G_{1,q+1}^\dagger(E) + G_{q,n}(E) \Sigma_R^{in}(E) G_{n,q+1}^\dagger(E) - G_{q+1,1}(E) \Sigma_L^{in}(E) G_{1,q}^\dagger(E) - G_{q+1,n}(E) \Sigma_R^{in}(E) G_{n,q}^\dagger(E)]. \quad (81)$$

The current density is given by

$$J_{q \rightarrow q+1} = \frac{ie\hbar}{2ma^2} 2 \int \frac{dE}{2\pi} [G(E) \Sigma_{lead}^{in}(E) G^\dagger(E) |_{q,q+1} - G(E) \Sigma_{lead}^{in}(E) G^\dagger(E) |_{q+1,q}]. \quad (82)$$

Electron correlation function: More generally, we define the electron correlation function G^n , which is the solution to

$$AG^n = \Sigma_{lead}^{in} G^\dagger. \quad (83)$$

Noting that $G = A^{-1}$, it is easy to obtain eqn. (72) $G^n = G \Sigma_{lead}^{in} G^\dagger$.

The expressions for electron [eqn. (72)] and current [eqn. (82)] densities at energy E , in the phase coherent case at finite applied biases can now be written as,

$$n_q(E) = 2 \frac{G_{q,q}^n(E)}{2\pi a}, \quad (84)$$

$$J_{q \rightarrow q+1}(E) = \frac{i e \hbar}{2 m a^2} 2 \frac{1}{2\pi} [G_{q,q+1}^n(E) - G_{q+1,q}^n(E)]. \quad (85)$$

That is, the diagonal and first off-diagonal elements of G^n are related to the electron and current densities respectively. Note that these equations are entirely equivalent to eqns. (26) and (27) appearing in the Landauer-Buttiker approach.

Hole correlation function: In the absence of phase breaking scattering, the Green's function (G) and the electron correlation function (G^n) are sufficient for device modeling. Scattering introduces the need for the hole correlation function (G^p), whose role will become clearer in section V D. While the less-than Green's function is directly proportional to the density of occupied states, the hole correlation function is proportional to the density of unoccupied states.

The density of unoccupied states at grid point q is also obtained by applying the Landauer-Buttiker formalism. For this, we simply replace the probability of finding an occupied state in the contact $f_{L,R}$ by the probability of finding an unoccupied state in the contact, $1 - f_{L,R}$, in eqn. (26). Then following the derivation leading to eqn. (26), we obtain:

$$h_q = 2 \int \frac{dE}{2\pi} \left[G_{q,1}(E) \Sigma_L^{out}(E) G_{1,q}^\dagger(E) + G_{q,n}(E) \Sigma_R^{out}(E) G_{n,q}^\dagger(E) \right] \cdot \frac{1}{a}, \quad (86)$$

$$h_q = 2 \int \frac{dE}{2\pi} G(E) \Sigma_{lead}^{out} G^\dagger(E)|_{q,q} \cdot \frac{1}{a}, \quad (87)$$

where, the only non zero elements of Σ_{lead}^{out} are,

$$\Sigma_{lead_{1,1}}^{out}(E) = \Sigma_L^{out}(E) = 2 t_{d,l} \frac{1}{t} \sin(k_l a) t_{l,d} (1 - f_L) = -2 \text{Im}[\Sigma_L(E)] [1 - f_L(E)] \quad (88)$$

$$\Sigma_{lead_{n,n}}^{out}(E) = \Sigma_R^{out}(E) = 2 t_{d,r} \frac{1}{t} \sin(k_r a) t_{r,d} (1 - f_R) = -2 \text{Im}[\Sigma_R(E)] [1 - f_R(E)]. \quad (89)$$

Akin to Eqs. (83) and (84), the density of unoccupied states at energy E , at grid point q can be expressed as the diagonal elements of G^p ,

$$h_q(E) = 2 \frac{G_{q,q}^p(E)}{2\pi a}, \quad (90)$$

where, G^p is in general given by,

$$A G^p = \Sigma_{lead}^{out} G^\dagger. \quad (91)$$

D. Electron-phonon scattering

In section V C, we defined the retarded, in-scattering and out-scattering self-energies in the device arising from coupling of the device to the external contacts. The self-energy Σ_L^{in} represents in-scattering of electrons (in-scattering rate) from the semi-infinite left contact to the device, assuming that grid point 1 of the device is empty. A similar statement applies to Σ_R^{in} . The in-scattering self-energy of the contacts depend on their Fermi distribution functions and surface density of states.

A second source for in-scattering to grid point q and energy E [(q, E)] is electron-phonon interaction. The self-energy at (q, E) has two terms corresponding to in-scattering from $(q, E + \hbar\omega_{phonon})$ and $(q, E - \hbar\omega_{phonon})$, as shown in Fig. 7. Intuitively, the in-scattering self-energy (in-scattering rate) at (x, E) should depend on the Bose factor for phonon occupancy, the deformation potential for electron-phonon scattering and the availability of electrons at energies $E + \hbar\omega_{phonon}$ and $E - \hbar\omega_{phonon}$. It follows rigorously, within the Born approximation that the in-scattering

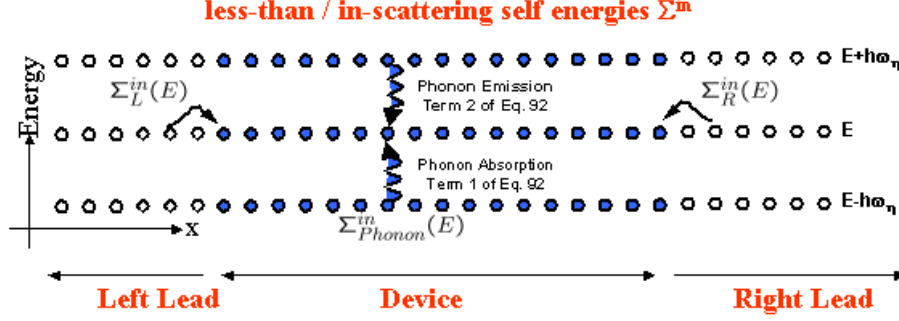


FIG. 7: Pictorial representation of the meaning the two in-scattering self-energies that appear in this chapter. $\Sigma_L^{in}(E)$ and $\Sigma_R^{in}(E)$ are the self-energies of the leads, and are non-zero only at the first and last Device grid points. $\Sigma_{Phonon}^{in}(E)$ is the self-energy due to electron-phonon interaction, and is non-zero at all Device grid points.

self energy into a fully empty state at energy E and grid point q is [Mah87]

$$\Sigma_{inel,q}^{in}(E) = \sum_{\eta} D_q^{\eta} \left[n_B(\hbar\omega_{phonon}) G_q^n(E - \hbar\omega_{phonon}) + (n_B(\hbar\omega_{phonon}) + 1) G_q^n(E + \hbar\omega_{phonon}) \right]. \quad (92)$$

D_q^{η} represents the electron-phonon scattering strength at grid point q . The first term of eqn. (92) represents in-scattering to E from $E - \hbar\omega_{phonon}$ (phonon absorption). n_B is the Bose distribution function for phonons of energy $\hbar\omega_{phonon}$ and $G_q^n(E - \hbar\omega_{phonon})$ is the electron density at $E - \hbar\omega_{phonon}$. The first and second terms of eqn. (92) represents in-scattering of electrons from $E - \hbar\omega_{phonon}$ (phonon absorption) and $E + \hbar\omega_{phonon}$ (phonon emission) to E respectively. The in-scattering rate at grid point q is given by

$$\text{In-scattering rate at grid point } q: \frac{\hbar}{\tau_q^{in}(E)} = \Sigma_q^{in}(E), \quad (93)$$

where Σ_q^{in} is the sum of all in-scattering self energies at grid point q .

The out-scattering self-energy Σ_L^{out} in eqn. (88) represents out-scattering of electrons from grid point 1 in the device to the semi-infinite left contact, assuming that grid point 1 of the device was occupied. The out-scattering self-energy due to the left contact Σ_L^{out} depends on the probability of finding an unoccupied state in the left contact $1 - f_L$ and the surface density of states of the left contact. A similar statement applies to Σ_R^{out} . A second source for out-scattering of electrons from an occupied state at (q, E) is electron-phonon interaction, which leads to scattering to $(q, E + \hbar\omega_{phonon})$ and $(q, E - \hbar\omega_{phonon})$ as represented in Fig. 8. Intuitively, the out-scattering self-energy (out-scattering rate) at (q, E) should depend on the Bose factor for phonon occupancy, the deformation potential for electron-phonon scattering and the availability of unoccupied states at energies $E + \hbar\omega_{phonon}$ and $E - \hbar\omega_{phonon}$. It follows rigorously, within the Born approximation that the out-scattering self energy from a fully filled state at (q, E) is [Mah87]

$$\Sigma_{Phonon,q}^{out}(E) = \sum_{\eta} D_q^{\eta} \left[(n_B(\hbar\omega_{phonon}) + 1) G_q^p(E - \hbar\omega_{phonon}) + n_B(\hbar\omega_{phonon}) G_q^p(E + \hbar\omega_{phonon}) \right]. \quad (94)$$

In the above equation, $G_q^p(E - \hbar\omega_{phonon})$ and $G_q^p(E + \hbar\omega_{phonon})$ are the densities of unoccupied states at $E - \hbar\omega_{phonon}$ and $E + \hbar\omega_{phonon}$. So the first and second terms of eqn. (94) represents out-scattering of electrons from E to $E + \hbar\omega_{phonon}$ (phonon emission) and $E - \hbar\omega_{phonon}$ (phonon absorption) respectively. The out-scattering rate at grid point q is given by

$$\text{Out-scattering rate at grid point } q: \frac{\hbar}{\tau_q^{out}(E)} = \Sigma_q^{out}(E), \quad (95)$$

where Σ_q^{out} is the sum of all out-scattering self energies at grid point q .

We now discuss how the in-scattering self-energy due to electron-phonon scattering affects the expression for electron density. The electron density at grid point q in the phase-coherent case (eqn. (72)) is the sum of two terms,

$$n_q = 2 \int \frac{dE}{2\pi} \left[G_{q,1}(E) \Sigma_L^{in}(E) G_{1,q}^{\dagger}(E) + G_{q,1}(E) \Sigma_R^{in}(E) G_{1,q}^{\dagger}(E) \right] \cdot \frac{1}{a}. \quad (96)$$

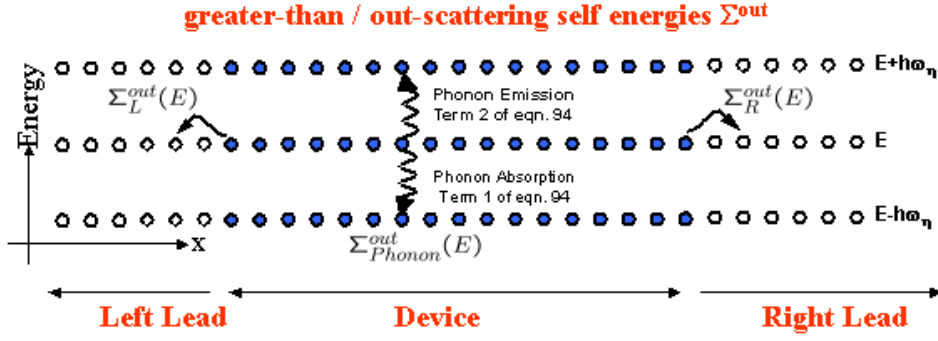


FIG. 8: Pictorial representation of the meaning the two out-scattering self-energies that appear in this chapter. $\Sigma_{lead_q}^{out}(E)$ is self-energy due to leads, which is non-zero only at the first and last Device grid points $\Sigma_{Phonon_q}^{out}(E)$ is self-energy due to electron-phonon interaction, which is non-zero at all Device grid points.

The first term represents in-scattering of electrons from the left contact [$(\Sigma_L^{in}(E))$], which is propagated to grid point q via the term $G_{q,1}(E)G_{1,q}^\dagger(E)$. The interpretation of the second term is similar except that it involves the right contact. In the presence of electron-phonon interaction, the in-scattering functions Σ_{Phonon}^{in} is non zero at all grid points. As a result, an electron can scatter from (q', E') to (q', E) and then propagate to grid point (q, E) via the term $G_{q,q'}(E)G_{q',q}^\dagger(E)$. The expression for the electron density can be generalized to include such terms,

$$\begin{aligned} n_q &= 2 \int \frac{dE}{2\pi} \left[G_{q,1}(E)\Sigma_L^{in}(E)G_{1,q}^\dagger(E) + G_{q,1}(E)\Sigma_R^{in}(E)G_{1,q}^\dagger(E) + \sum_{q'} G_{q,q'}(E)\Sigma_{q',Phonon}^{in}(E)G_{q',q}^\dagger(E) \right] \cdot \frac{1}{a} \\ &= 2 \int \frac{dE}{2\pi} [G(E)\Sigma_{lead}^{in}(E)G^\dagger(E) + G(E)\Sigma_{Phonon}^{in}(E)G^\dagger(E)]|_{q,q} \cdot \frac{1}{a} \\ &= 2 \int \frac{dE}{2\pi} G_{q,q}^n(E) \cdot \frac{1}{a} \end{aligned} \quad (97)$$

where the third term corresponds to propagation of electrons from grid point q' to q after a scattering event at q' as shown in Fig. (9). The in-scattering self energies due to phonon scattering are given by eqn. (92). More generally, G^n is given by,

$$G^n(E) = G(E)\Sigma^{in}(E)G^\dagger(E) \quad (98)$$

$$[E - H - \Sigma(E)]G^n(E) = \Sigma^{in}(E)G^\dagger(E), \quad (99)$$

where Σ^{in} is the sum of self-energies due to leads, electron-phonon interaction and all other processes. The reader can compare the above two equations to Eqs. (73) and (83), which are valid in the phase coherent limit.

The density of unoccupied states can be written in a manner identical to eqn. (97) as,

$$\begin{aligned} h_q &= 2 \int \frac{dE}{2\pi} \left[G_{q,1}(E)\Sigma_L^{out}(E)G_{1,q}^\dagger(E) + G_{q,1}(E)\Sigma_R^{out}(E)G_{1,q}^\dagger(E) + \sum_{q'} G_{q,q'}(E)\Sigma_{q',Phonon}^{out}(E)G_{q',q}^\dagger(E) \right] \cdot \frac{1}{a} \\ &= 2 \int \frac{dE}{2\pi} [G(E)\Sigma_{lead}^{out}(E)G^\dagger(E) + G(E)\Sigma_{Phonon}^{out}(E)G^\dagger(E)]|_{q,q} \cdot \frac{1}{a} \\ &= 2 \int \frac{dE}{2\pi} G_{q,q}^p(E) \cdot \frac{1}{a}. \end{aligned} \quad (100)$$

More generally, the G^p matrix is given by,

$$G^p(E) = G(E)\Sigma^{out}(E)G^\dagger(E) \quad (101)$$

$$[E - H - \Sigma(E)]G^p(E) = \Sigma^{out}(E)G^\dagger(E), \quad (102)$$

where Σ^{out} is the sum of self-energies due to leads, electron-phonon interaction and all other processes.

Three contributions to electron density in eqn. 97

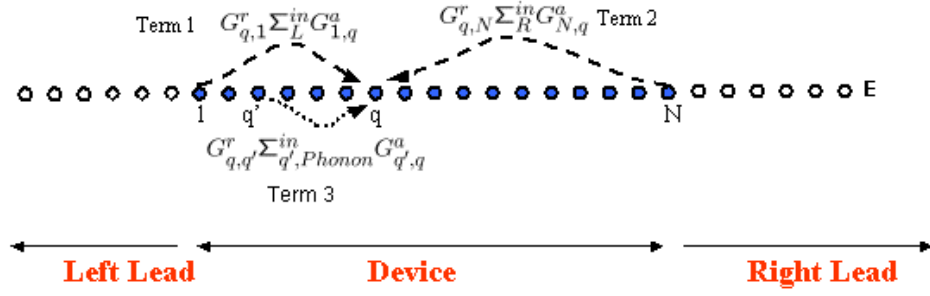


FIG. 9: Contributions to electron density from leads and electron-phonon scattering.

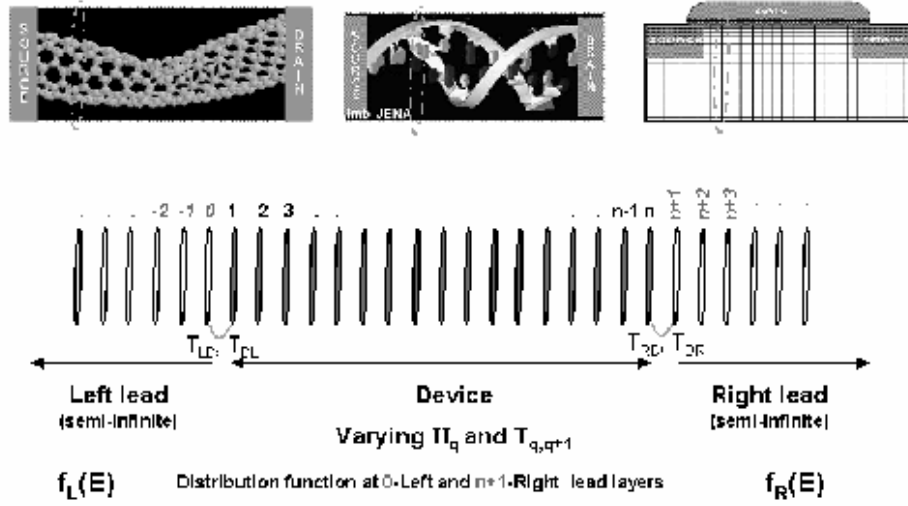


FIG. 10: (Top) Examples of the layered structures: carbon nanotube, DNA molecule, MOSFET. (Bottom) Scheme of simulation domains in the layered structure: device, left and right leads.

Note that in general G^n and G^p are full matrices, the diagonal elements of which correspond to density of occupied and unoccupied states respectively, and the first off diagonal elements of G^n and G^p correspond to the current density. The Green's function G in the device region is obtained by solving,

$$[E - H - \Sigma_{lead}(E) - \Sigma_{Phonon}(E)]G = I, \quad (103)$$

which is similar to eqn. (60) for the phase coherent case, except for the additional self-energy due to phonon scattering.

VI. NON-EQUILIBRIUM GREEN'S FUNCTION EQUATIONS FOR LAYERED STRUCTURES

The previous section dealt with a simple one dimensional Hamiltonian. In this section, we will present the NEGF equations for a family of more realistic structures called *layered structures*. A layer can be considered to be a generalization of a single grid points / orbital (Fig. 6) to a set of grid point / orbitals (Fig. 10). Three examples of layered structures are shown in Fig. 10. The left most figure is a carbon nanotube, the middle figure is a DNA strand and the right figure is a MOSFET. A *layer* consists of the atoms / grid points between the dashed lines in Fig. 10.

A common approximation used to describe the Hamiltonian of layered structures consists of interaction only between nearest neighbor layers. That is, each layer q interacts only with itself and its nearest neighbor layers $q - 1$ and $q + 1$. Then, the single particle Hamiltonian of the layered structure is a block tridiagonal matrix, where diagonal blocks H_q

are the coupling between the Left and Right leads and Device respectively. Note that $A'_{DL} = A'_{LD}^\dagger$, $A'_{DR} = A'_{RD}^\dagger$, and A'_{LD} and A'_{DL} (A'_{RD} , and A'_{DR}) are sparse matrices. Their only non-zero entry represents coupling between the Left (Right) lead and Device. O represents zero matrices. From eqn. (107), we have:

$$G_{LD} = -A'^{-1}_{LL} A'_{LD} G_{DD} \quad (112)$$

$$G_{RD} = -A'^{-1}_{RR} A'_{RD} G_{DD} \quad (113)$$

$$A'_{DL} G_{LD} + A'_{DD} G_{DD} + A'_{DR} G_{RD} = I . \quad (114)$$

Substituting Eqs. (112) and (113) in eqn. (114), we obtain a matrix equation with dimension corresponding to total number of grid points / orbitals in the n device layers ,

$$[A'_{DD} - A'_{DL} A'^{-1}_{LL} A'_{LD} - A'_{DR} A'^{-1}_{RR} A'_{RD}] G_{DD} = I . \quad (115)$$

The second and third terms of eqn. (115) are self energies due to coupling of the Device region to Left and Right leads respectively.

The Green's functions of the isolated semi-infinite leads by definition are,

$$A'_{LL} g_L = I \text{ and } A'_{RR} g_R = I . \quad (116)$$

The **surface Green's function** of the Left and Right leads are the Green's function elements corresponding to the edge layers -1 and $n+1$ respectively,

$$g_{L_{-1,-1}} = A'^{-1}_{LL_{1,1}} \text{ and } g_{R_{n+1,n+1}} = A'^{-1}_{RR_{1,1}} . \quad (117)$$

Eq. (115) can now be rewritten in a form very similar to eqn. (60),

$$[EI - H - \Sigma_{Phonon} - \Sigma_{lead}] G_{DD} = I \quad (118)$$

where,

$$\Sigma_{lead1,1} = T_{DL} g_{L_{-1,-1}} T_{LD} = \Sigma_L \quad (119)$$

$$\Sigma_{leadn,n} = T_{DR} g_{R_{n+1,n+1}} T_{RD} = \Sigma_R . \quad (120)$$

All other elements of Σ_{lead} are zero. Σ_L and Σ_R are **self-energies** due to the Left and Right leads respectively, and $T_{DL} = T^\dagger_{LD}$ and $T_{DR} = T^\dagger_{RD}$. Finally, defining,

$$A_{DD} = EI - H - \Sigma_{Phonon} - \Sigma_{lead} , \quad (121)$$

eqn. (118) can be written as

$$A_{DD} G_{DD} = I . \quad (122)$$

The main information needed to solve eqn. (118) are the surface Green's functions of g_L and g_R . We will discuss two methods to obtain this surface Green's functions for a constant potential in the Left and Right leads. When the potential does not vary, A'_{LL} and A'_{RR} are semi-infinite periodic matrices with all diagonal / off-diagonal blocks being equal:

$$A_{l1} = A_{l2} = A_{l3} = \dots = A_l \quad (123)$$

$$T_{l1} = T_{l2} = T_{l3} = \dots = T_l . \quad (124)$$

$g_{L_{-1,-1}}$ is obtained by solving the matrix quadratic equation:

$$[A_l - T_l^\dagger g_{L_{-1,-1}} T_l] g_{L_{-1,-1}} = I . \quad (125)$$

This equation can be solved iteratively by,

$$[A_l - T_l^\dagger g_{L_{-1,-1}}^{<m-1>} T_l] g_{L_{-1,-1}}^{<m>} = I , \quad (126)$$

where, the superscript of g_L represents the iteration number. Note that the solution to eqn. (125) is analytic when the dimension of A_l is one. A second simpler solution to obtain g_L involves transforming to an eigen mode basis using an unitary transformation (S), such that

$$S^{-1} A_l S = A_{ld} \text{ and } S^{-1} T_l S = T_{ld} , \quad (127)$$

where, both A_{ld} and T_{ld} are diagonal matrices. The surface Green's function in this new basis is simply a diagonal matrix, whose elements are obtained by solving the scalar quadratic version of eqn. (125). The Green's function in the original basis (in which A_l is not diagonal) can be obtained using the inverse unitary transformation.

Electron (G^n) and Hole (G^p) Green's Function:

The electron density is equal to [see the discussion of electron density in section V C],

$$n(\vec{r}, E) = 2 \frac{G^n(\vec{r}, \vec{r}, E)}{2\pi} . \quad (128)$$

The governing equation for G^n is

$$[EI - H - \Sigma_{Phonon}]G^n = \Sigma_{Phonon}^{in}G^\dagger , \quad (129)$$

where G^\dagger is the hermitian conjugate Green's function and Σ_{Phonon}^{in} is the in-scattering self-energy due to phonon scattering. The dimension of Eq. (129) is essentially infinite due to the semi-infinite Left and Right leads. It can however be converted to a finite dimensional matrix with dimension equal to the number of grid points / orbitals corresponding to the n device layers. In a manner identical to the derivation of eqn. (118) for the retarded Green's function, it can be shown that the role of the leads can be folded into layers 1 and n to yield,

$$[EI - H - \Sigma_{Phonon} - \Sigma_{lead}]G_{DD}^n = \Sigma_{DD}^{in}G_{DD}^\dagger . \quad (130)$$

or

$$A_{DD}G_{DD}^n = \Sigma_{DD}^{in}G_{DD}^\dagger , \quad (131)$$

where A_{DD} has been defined in eqn. (121). The self-energy Σ_{DD}^{in} has contributions due to both electron-phonon interaction and leads,

$$\Sigma_{DD_{1,1}}^{in} = \Sigma_{Phonon_{1,1}}^{in} + \Sigma_L^{in} \quad (132)$$

$$\Sigma_{DD_{n,n}}^{in} = \Sigma_{Phonon_{n,n}}^{in} + \Sigma_R^{in} \quad (133)$$

$$\Sigma_{DD_{q,q}}^{in} = \Sigma_{Phonon_{q,q}}^{in} , \text{ where, } q=2, 3, 4, \dots n-1. \quad (134)$$

The **in-scattering self-energies** due to the leads, Σ_L^{in} and Σ_R^{in} have forms very similar to eqns. (70) and (71) of section V C,

$$\Sigma_L^{in}(E) = -2 \text{Im}[\Sigma_L(E)]f_L(E) = \Gamma_L(E)f_L(E) \quad (135)$$

$$\Sigma_R^{in}(E) = -2 \text{Im}[\Sigma_R(E)]f_R(E) = \Gamma_R(E)f_R(E) , \quad (136)$$

where,

$$\Gamma_L(E) = -2 \text{Im}[\Sigma_L(E)] \quad (137)$$

$$\Gamma_R(E) = -2 \text{Im}[\Sigma_R(E)] . \quad (138)$$

f_L and f_R are the distribution functions in the Left and Right leads respectively (Fermi factors at equilibrium). The self-energies $\Sigma_L(E)$ and $\Sigma_R(E)$ have been defined in eqn. (119) and (120).

The diagonal elements of the hole correlation functions $G^p(E)$ represents the density of unoccupied states,

$$h(\vec{r}, E) = 2 \frac{G^p(\vec{r}, \vec{r}, E)}{2\pi} . \quad (139)$$

The governing equation for $G^p(E)$ is,

$$[EI - H - \Sigma_{Phonon}]G^p = \Sigma_{Phonon}^{out}G^\dagger \quad (140)$$

or

$$A_{DD}G_{DD}^p = \Sigma_{DD}^{out}G_{DD}^\dagger \quad (141)$$

$$\Sigma_{DD_{11}}^{out} = \Sigma_{Phonon_{11}}^{out} + \Sigma_L^{out} \quad (142)$$

$$\Sigma_{DD_{nn}}^{out} = \Sigma_{Phonon_{nn}}^{out} + \Sigma_R^{out} \quad (143)$$

$$\Sigma_{DD_{ii}}^{out} = \Sigma_{Phonon_{ii}}^{out} , \text{ where, } i=2, 3, 4, \dots n-1 \quad (144)$$

where Σ_{Phonon}^{out} is the out-scattering self-energy due to phonon scattering. The **out-scattering self-energies** due to the leads, Σ_L^{out} and Σ_R^{out} have forms very similar to eqns. (88) and (89)

$$\Sigma_L^{out}(E) = -2 \text{Im}[\Sigma_L(E)](1 - f_L(E)) = \Gamma_L(1 - f_L(E)) \quad (145)$$

$$\Sigma_R^{out}(E) = -2 \text{Im}[\Sigma_R(E)](1 - f_R(E)) = \Gamma_R(1 - f_R(E)) , \quad (146)$$

where $1 - f_L(E)$ ($1 - f_R(E)$) is the probability of finding an unoccupied state in the left (right) contact at energy E . Eqns. (131) and (141) for G^n and G^p can be written as,

$$G_{DD}^n = A_{DD}^{-1} \Sigma_{DD}^{in} G_{DD}^\dagger = G_{DD} \Sigma_{DD}^{in} G_{DD}^\dagger \quad (147)$$

$$G_{DD}^p = A_{DD}^{-1} \Sigma_{DD}^{out} G_{DD}^\dagger = G_{DD} \Sigma_{DD}^{out} G_{DD}^\dagger . \quad (148)$$

While these equations appear often in literature, we do not suggest using them to compute the diagonal elements of G^n and G^p of layered structures. This is because their use requires knowledge of the entire G_{DD} matrix when Σ_{DD}^{in} is non zero at all grid points. Computation of the entire G_{DD} amounts to inversion of A_{DD} . Matrix inversion is computationally expensive and scales as $N^{2.7}$ where N is the dimension of A_{DD} . The diagonal elements of G^n and G^p of layered structures can be computed more efficiently without calculating the entire G_{DD} matrix using the algorithm discussed in appendix C.

Current Density: We will now present some expression for current density commonly used in literature. The current flowing between layers q and $q + 1$ is (eqn. (85) of section V C):

$$J_{q \rightarrow q+1} = \frac{ie}{\hbar} 2 \int \frac{dE}{2\pi} \text{Tr} [T_{q,q+1} G_{q+1,q}^n(E) - T_{q+1,q} G_{q,q+1}^n(E)] . \quad (149)$$

Eq. (149) frequently appears in the literature in other useful forms that are derived below. Expanding both terms of eqn. (149) using eqn. (C10) of appendix B, we get,

$$J_L = \frac{ie}{\hbar} 2 \int \frac{dE}{2\pi} \text{Tr} ([T_{LD} G_{1,1}(E) T_{DL} g_{L_{0,0}}^n(E) + T_{LD} G_{1,1}^n(E) T_{DL} g_{L_{0,0}}^\dagger(E) - [T_{DL} G_{L_{0,0}}^m(E) T_{LD} G_{1,1}^\dagger(E) + T_{DL} g_{L_{0,0}}^\dagger(E) T_{LD} G_{1,1}^n(E)])] \quad (150)$$

$$= \frac{ie}{\hbar} 2 \int \frac{dE}{2\pi} \text{Tr} ([G_{1,1}(E) - G_{1,1}^\dagger(E)] T_{DL} g_{L_{0,0}}^n(E) T_{LD} - G_{1,1}^n(E) T_{DL} [g_{L_{0,0}}(E) - g_{L_{0,0}}^\dagger(E)] T_{LD}) \quad (151)$$

Using the relationships,

$$\Sigma_L^{in} = T_{DL} g_{L_{0,0}}^n T_{LD} \quad (152)$$

$$-i\Gamma_L = T_{DL} [g_{L_{0,0}} - g_{L_{0,0}}^\dagger] T_{LD} , \quad (153)$$

Eq. (151) can be written as,

$$J_L = \frac{e}{\hbar} 2 \int \frac{dE}{2\pi} \text{Tr} (i[G_{1,1}(E) - G_{1,1}^\dagger(E)] \Sigma_L^{in}(E) - G_{1,1}^n(E) \Gamma_L(E)) \quad (154)$$

Eqns. (149) and (154) are both general expression for current density valid in the presence of electron-phonon scattering in the device [Mei90]. The advantage of using eqn. (149) is that the current density can be calculated at every layer in the device. This expression is useful in understanding how the current density is energetically redistributed along the length of the device as a result of scattering.

In the phase coherent limit, $\Sigma_{Phonon} = 0$ and the only non zero self-energies are in layers 1 and n due to the contacts. We define matrices, $\tilde{\Gamma}_L$ and $\tilde{\Gamma}_R$, which consist of n blocks corresponding to the n Device layers (dimension of A_{DD} matrix) and with the following non zero elements:

$$\tilde{\Gamma}_L|_{1,1} = \Gamma_L, \quad \tilde{\Gamma}_R|_{n,n} = \Gamma_R . \quad (155)$$

Now left multiplying eqn. (122) by G^\dagger and right multiplying the Hermitian conjugate of eqn. (122) by G , and subtracting the resulting two equations, we have,

$$G - G^\dagger = G^\dagger (\Sigma - \Sigma^\dagger) G , \quad (156)$$

where Σ is the total self-energy due to phonons and the leads. The Hermitean conjugate Green's functions and self-energies are G^\dagger and Σ^\dagger . In the absence of phonon scattering, the self energies only have components due to the leads and so eqn. (156) can be written as,

$$i[G - G^\dagger] = G^\dagger(\tilde{\Gamma}_L + \tilde{\Gamma}_R)G, \text{ where} \quad (157)$$

eqns. (137) and (138) have been used. It also follows from Eqs. (135), (136) and (147) that

$$G^n = G(\tilde{\Gamma}_L f_L + \tilde{\Gamma}_R f_R)G^\dagger. \quad (158)$$

Now using eqns. (157) and (158) in eqn. (154), the current in the phase coherent limit is,

$$J_L = \frac{e}{\hbar} 2 \int \frac{dE}{2\pi} T(E) [f_L(E) - f_R(E)]. \quad (159)$$

The total transmission at energy E is identified from eqn. (159) to be

$$T(E) = \text{Tr}[\tilde{\Gamma}_L(E)G(E)\tilde{\Gamma}_R(E)G^\dagger(E)]. \quad (160)$$

Note that to compute the total transmission using eqn. (160), only the elements of G connecting layers 1 and n are required because $\tilde{\Gamma}_L$ and $\tilde{\Gamma}_R$ are non zero only in layers 1 and n respectively.

A. Crib Sheet

The algorithmic flow in modeling nanodevices using the non equilibrium Green's function consists of the following steps (Fig. 11). We first find a guess for the electrostatic potential $V(\vec{r})$ and calculate the self energies due to the contacts (eqns. (175) - (185)). The self-energies due to electron-phonon scattering are set to zero. The non equilibrium Green's function equations for G , G^n and G^p (eqs. (171) - eqs(174)) are then solved. Following this, the self energies due to electron phonon scattering and contacts (eqns. (175) - (185)) are calculated. As the equations governing the Green's functions depend on the self energies, we iteratively solve for the Green's function and self-energies, as indicated by the inner loop of Fig. 11. Then, the electron density (diagonal elements of G^n) is used in Poisson's equation to obtain a new potential profile. We use this updated electrostatic potential profile as an input to solve for updated non equilibrium Green's functions, and continue the above process iteratively until convergence is achieved (outer loop of Fig. 11). A number of equations that are repeatedly used in nanodevice modeling are listed below.

Physical Quantities:

$$\text{Scattering Rate: } \frac{\hbar}{\tau(E)} = -2 \text{Im}[\Sigma(E)] = \Gamma(E) \quad (161)$$

$$(162)$$

$$\text{Density of States at } (\vec{r}, E): \quad N(\vec{r}, E) = -\frac{1}{\pi} \text{Im}(G(\vec{r}, \vec{r}, E)) \quad (163)$$

Use recursive algorithm to calculate DOS (Do not invert A).

$$\text{Electron / Occupied density at } \vec{r}: \quad n(\vec{r}) = 2 \int \frac{dE}{2\pi} G^n(\vec{r}, \vec{r}, E) \quad (164)$$

Use recursive algorithm to calculate n (Do not use $G^n = G\Sigma^{in}G^\dagger$).

$$\text{Unoccupied Density at } \vec{r}: \quad h(\vec{r}) = 2 \int \frac{dE}{2\pi} G^p(\vec{r}, \vec{r}, E) \quad (165)$$

Use recursive algorithm to calculate h (Do not use $G^n = G\Sigma^{in}G^\dagger$).

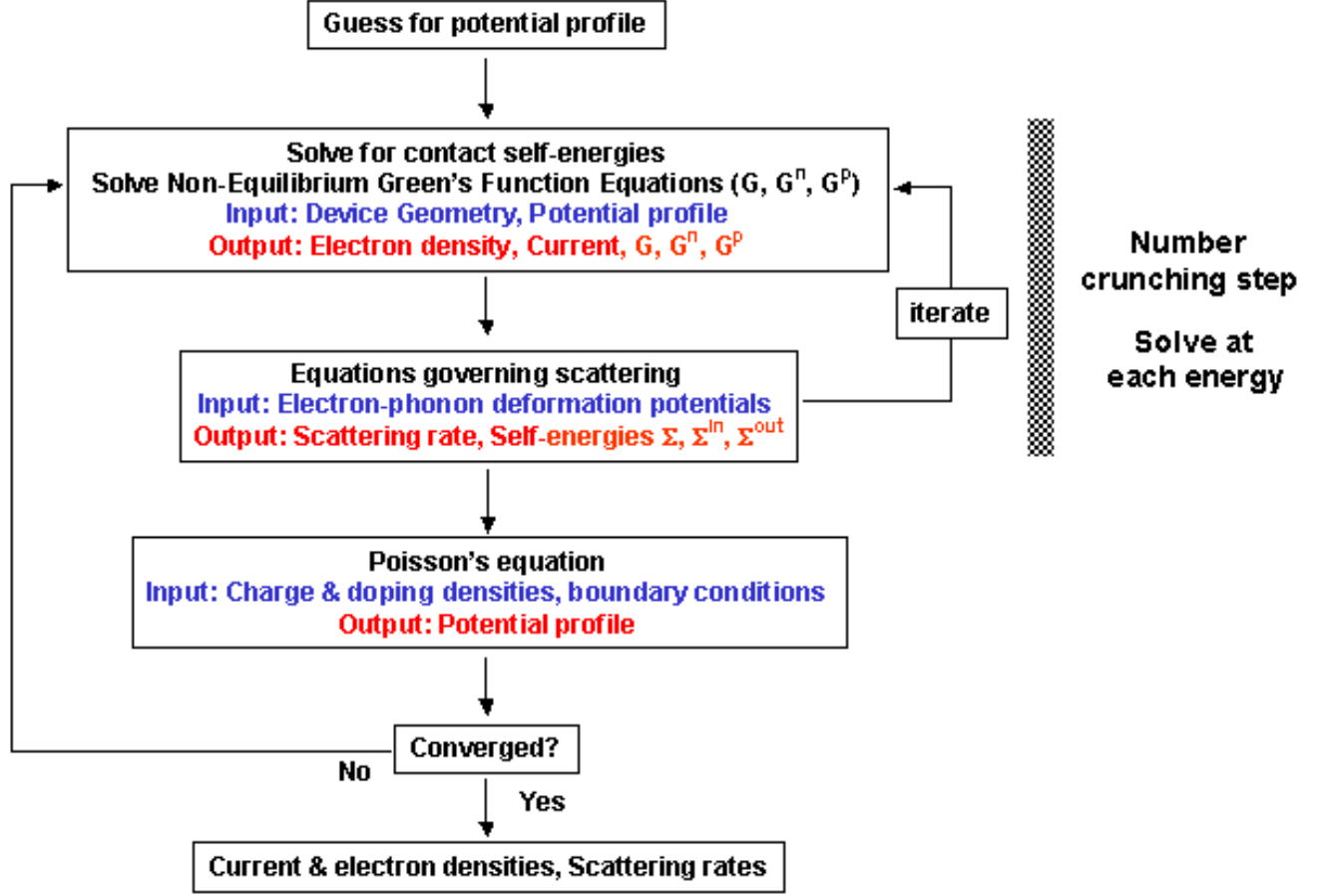


FIG. 11: Flowchart of a typical simulation involved in modeling of a nanodevice.

Current density flowing between layers q and $q + 1$ (valid with scattering in device):

$$J_{q \rightarrow q+1} = \frac{ie}{\hbar} 2 \int \frac{dE}{2\pi} \text{Tr} [T_{q,q+1} G_{q+1,q}^n(E) - T_{q+1,q} G_{q,q+1}^n(E)] \quad (166)$$

Current density flowing from the Left lead into layer 1 of Device (valid with scattering in device):

$$J_L = \frac{e}{\hbar} 2 \int \frac{dE}{2\pi} \text{Tr} \{ i [G_{1,1}(E) - G_{1,1}^\dagger(E)] \Sigma_L^{\text{in}}(E) - G_{1,1}^n(E) \Gamma_L(E) \} \quad (167)$$

$$= \frac{e}{\hbar} 2 \int \frac{dE}{2\pi} \text{Tr} \{ G_{1,1}^p(E) \Sigma_L^{\text{in}}(E) - G_{1,1}^n(E) \Sigma_L^{\text{out}}(E) \} \quad (168)$$

Current density flowing from the Left lead into layer 1 of Device (valid only in the phase coherent limit):

$$J_L = \frac{e}{\hbar} 2 \int \frac{dE}{2\pi} T(E) [f_L(E) - f_R(E)], \quad (169)$$

where the total transmission from the Left to Right lead at energy E is given by

$$T(E) = \text{Tr} [\tilde{\Gamma}_L(E) G(E) \tilde{\Gamma}_R(E) G^\dagger(E)]. \quad (170)$$

Only elements of G connecting layers 1 and n are necessary.

Equations Solved:

$$\text{Green's Function:} \quad [EI - H - \Sigma]G(E) = I \rightarrow AG = I \quad (171)$$

$$\text{Hermitean conjugate Green's Function:} \quad G^\dagger(E)[EI - H - \Sigma^\dagger] = I \quad (172)$$

$$\text{electron correlation Function:} \quad [EI - H - \Sigma]G^n(E) = \Sigma^{\text{in}}(E)G^\dagger(E) \rightarrow AG^n = \Sigma^{\text{in}}G^\dagger \quad (173)$$

$$\text{hole correlation Function:} \quad [EI - H - \Sigma]G^p(E) = \Sigma^{\text{out}}(E)G^\dagger(E) \rightarrow AG^p = \Sigma^{\text{out}}G^\dagger \quad (174)$$

$$\Sigma^\alpha(E) = \Sigma_{lead}^\alpha(E) + \Sigma_{Phonon}^\alpha(E), \text{ where } \alpha \in in, out \quad (175)$$

$$\Sigma_{lead_{1,1}}^\alpha = \Sigma_L^\alpha(E) = T_{DL} g_{L_{0,0}}^\alpha T_{LD} \quad (176)$$

$$\Sigma_{lead_{n,n}}^\alpha = \Sigma_R^\alpha(E) = T_{DR} g_{R_{n+1,n+1}}^\alpha T_{RD} \quad (177)$$

$$\Sigma_{lead_{i,i}}^\alpha = 0 \quad \forall \quad i \neq 1, n \quad (178)$$

$$\Gamma(E) = -2 \text{Im}[\Sigma(E)] \quad (179)$$

$$\Gamma_L(E) = -2 \text{Im}[\Sigma_L(E)] \quad (180)$$

$$\Gamma_R(E) = -2 \text{Im}[\Sigma_R(E)] \quad (181)$$

$$\Sigma_L^{in}(E) = \Gamma_L(E) f_L(E) \quad (182)$$

$$\Sigma_R^{in}(E) = \Gamma_R(E) f_R(E) \quad (183)$$

$$\Sigma_L^{out}(E) = \Gamma_L[1 - f_L(E)] \quad (184)$$

$$\Sigma_R^{out}(E) = \Gamma_R[1 - f_R(E)] \quad (185)$$

The diagonal and nearest neighbor off-diagonal elements of G and G^n are computed repeatedly as they correspond to physical quantities such as the density of states, electron density and current. Non local scattering mechanisms, which requires calculation of further off-diagonal elements, are not discussed here.

Useful Relationships:

$$i[G - G^\dagger] = G^p + G^n = \text{DOS} \quad (186)$$

$$i[\Sigma - \Sigma^\dagger] = \Sigma^{out} + \Sigma^{in} = \Gamma \quad (187)$$

$$G - G^\dagger = G[\Sigma^\dagger - \Sigma]G^\dagger \quad (188)$$

$$= G^\dagger[\Sigma^\dagger - \Sigma]G \quad (189)$$

$$= -iG\Gamma G^\dagger = -iG^\dagger\Gamma G \quad (190)$$

$$G^{n\dagger} = G^n \quad (191)$$

$$G^{p\dagger} = G^p \quad (192)$$

VII. APPLICATION TO A BALLISTIC NANOTRANSISTOR

Quantum mechanics is playing an increasingly important role in modeling transistors with channel lengths in the ten nanometer regime for many reasons: (i) **Tunneling** from gate to channel and source to drain determine the off current [Svi02]. (ii) **Ballistic** flow of electrons in the channel is important as the channel length becomes comparable to the electron mean free path. (iii) Classically, the electron distribution in the inversion layer is a sheet charge at the Si-SiO₂ interface. Quantum mechanically, the inversion layer charge is distributed over a few nanometers perpendicular to Si-SiO₂ interface due to **quantum confinement**. Methods based on the drift-diffusion and Boltzmann equations do not apriori capture the above mentioned quantum mechanical features.

In this section, we will discuss the equations involved in the two dimensional modeling of nanotransistors within the effective mass frame work [Ren03]. The quantum mechanical and semiclassical results are compared to illustrate their differences. The discretized matrix equations that we solve are discussed in section VII A. The application of the quantum mechanical method to illustrate the role of polysilicon gate depletion, and the slopes of I_d versus gate (V_g) and drain (V_d) voltages are discussed in section VII B.

Table 1. List of Abbreviations: Length Scales	
t_{ox}	oxide thickness
L_P	polysilicon gate thickness in x-direction
L_B	boundary of substrate region in x-direction
L_y	Poisson's and NEGF equations are solved from $-L_y/2$ to $+L_y/2$
L_g	length of polysilicon gate region in y-direction

A. Discretized equations

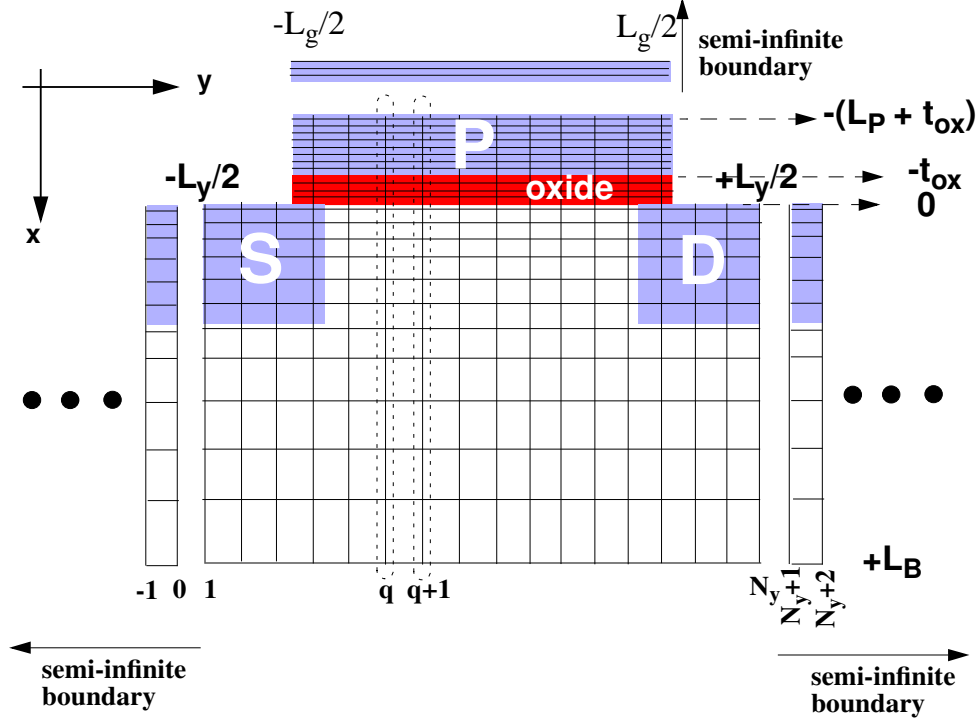


FIG. 12: The equations are solved in a two dimensional non uniform spatial grid, with semi-infinite boundaries as shown. Each column q corresponds to the diagonal blocks of the Green's function equations.

We consider N_b independent valleys for electrons within the effective mass approximation. The Hamiltonian of valley b is

$$H_b(\vec{r}) = -\frac{\hbar^2}{2} \left[\frac{d}{dx} \left(\frac{1}{m_x^b} \frac{d}{dx} \right) + \frac{d}{dy} \left(\frac{1}{m_y^b} \frac{d}{dy} \right) + \frac{d}{dz} \left(\frac{1}{m_z^b} \frac{d}{dz} \right) \right] + V(\vec{r}), \quad (193)$$

where (m_x^b, m_y^b, m_z^b) are components of effective mass in valley b . The equation of motion for the Green's function (G) and electron correlation function (G^n) are

$$[E - H_{b_1}(\vec{r}_1)]G_{b_1, b_2}(\vec{r}_1, \vec{r}_2, E) - \int d\vec{r} \Sigma_{b_1, b'}(\vec{r}_1, \vec{r}, E)G_{b', b_2}(\vec{r}, \vec{r}_2, E) = \delta_{b_1, b_2} \delta(\vec{r}_1 - \vec{r}_2) \quad (194)$$

and

$$[E - H_{b_1}(\vec{r}_1)]G_{b_1, b_2}^{n(p)}(\vec{r}_1, \vec{r}_2, E) - \int d\vec{r} \Sigma_{b_1, b'}(\vec{r}_1, \vec{r}, E)G_{b', b_2}^{n(p)}(\vec{r}, \vec{r}_2, E) = \int d\vec{r} \Sigma_{b_1, b'}^{in(out)}(\vec{r}_1, \vec{r}, E)G_{b', b_2}^\dagger(\vec{r}, \vec{r}_2, E). \quad (195)$$

The coordinate spans only the device in Eqs. (194) and (195). The influence of the semi-infinite source (S), drain (D) and polysilicon gate (P) leads, and electron-phonon interaction are included via self-energy terms $\Sigma_{b_1, b'}$ and $\Sigma_{b_1, b'}^{in(out)}$ as discussed in section VI. The contact self-energies are diagonal in the band index, $\Sigma_{b_1, b_2, C}^\alpha = \Sigma_{b_1, C}^\alpha \delta_{b_1, b_2}$ (C represents contacts).

The electrostatic potential varies in the (x, y) plane of Fig. 12, and the system is translationally invariant along the z -axis. So, all quantities $A(\vec{r}_1, \vec{r}_2, E)$ depend only on the difference coordinate $z_1 - z_2$. Using the relation

$$A(\vec{r}_1, \vec{r}_2, E) = \int \frac{dk_z}{2\pi} e^{ik_z(z_1 - z_2)} A(x_1, y_1, x_2, y_2, k_z, E), \quad (196)$$

the equations of motion for G and $G^{n(p)}$ simplify to

$$\left[E - \frac{\hbar^2 k_z^2}{2m_z} - H_b(\vec{r}_1)\right]G_b(\vec{r}_1, \vec{r}_2, k_z, E) - \int d\vec{r} \Sigma_b(\vec{r}_1, \vec{r}, k_z, E)G_b(\vec{r}, \vec{r}_2, k_z, E) = \delta(\vec{r}_1 - \vec{r}_2) \quad (197)$$

and

$$\left[E - \frac{\hbar^2 k_z^2}{2m_z} - H_b(\vec{r}_1)\right]G_b(\vec{r}_1, \vec{r}_2, k_z, E) - \int d\vec{r} \Sigma_b(\vec{r}_1, \vec{r}, k_z, E)G_b^{n(p)}(\vec{r}, \vec{r}_2, k_z, E) = \int d\vec{r} \Sigma_b^{in(out)}(\vec{r}_1, \vec{r}, k_z, E)G_b^\dagger(\vec{r}, \vec{r}_2, k_z, E), \quad (198)$$

where $Z_b = Z_{b,b}$, and $\vec{r} \rightarrow (x, y)$ for the remainder of this section.

Eqs. (197) and (198) can be written in matrix form as,

$$A'G = \lambda \text{ and} \quad (199)$$

$$\text{and} \quad A'G^{n(p)} = \Sigma^{in(out)}G^\dagger. \quad (200)$$

The self-energies due to S, D and P are non zero only along the lines $y = y_S = y_1$, $y = y_D = y_{N_y}$ and $x = -(L_P + t_{ox})$ respectively of Fig. 12. The A' matrix is ordered such that all grid points at a y -coordinate (layer) correspond to a diagonal block of dimension N_x , and there are N_y such blocks. In the notation adopted $A'_{j_1, j_2}(i, i')$ is the off-diagonal entry corresponding to grid points (x_i, y_{j_1}) and $(x_{i'}, y_{j_2})$. The non zero elements of the diagonal blocks of the A' matrix are

$$A'_{j,j}(i, i) = E' - V_{i,j} - T_{j,j}(i+1, i) - T_{j,j}(i-1, i) - T_{j+1,j}(i, i) - T_{j-1,j}(i, i) - \Sigma_S(x_i, x_i)\delta_{j,1} - \Sigma_D(x_i, x_i)\delta_{j, N_y} - \Sigma_P(y_j, y_j)\delta_{i,1} - \Sigma(x_i, y_j; x_i, y_j) \quad (201)$$

$$A'_{j,j}(i \pm 1, i) = T_{j,j}(i \pm 1, i) - \Sigma_S(x_{i \pm 1}, x_i)\delta_{j,1} - \Sigma_D(x_{i \pm 1}, x_i)\delta_{j, N_y} - \Sigma(x_{i \pm 1}, y_j; x_i, y_j) \quad (202)$$

$$A'_{j,j}(i, i') = -\Sigma_S(x_i, x_{i'})\delta_{j,1} - \Sigma_D(x_i, x_{i'})\delta_{j, N_y}, \text{ for } i' \neq i, i \pm 1, \quad (203)$$

where $E' = E - \hbar^2 k_z^2 / 2m_z$ and $V_{i,j} = V(x_i, y_j)$. The off-diagonal blocks are

$$A'_{j \pm 1, j}(i, i) = T_{j \pm 1, j}(i, i) - \Sigma_P(y_j, y_{j \pm 1})\delta_{i,1} \\ A'_{j, j'}(i, i') = 0, \text{ for } j' \neq j, j \pm 1, \quad (204)$$

and the non zero elements of the T matrix are

$$T_{j,j}(i \pm 1, i) = \frac{\hbar^2}{2m^{\pm x}} \frac{2}{x_{i+1} - x_{i-1}} \frac{1}{|x_{i \pm 1} - x_i|} \quad (205)$$

$$T_{j \pm 1, j}(i, i) = \frac{\hbar^2}{2m^{\pm y}} \frac{2}{y_{j+1} - y_{j-1}} \frac{1}{|y_{j \pm 1} - y_j|}, \quad (206)$$

where $m^{\pm x} = \frac{m_{i \pm 1, j} + m_{i, j}}{2}$ and $m^{\pm y} = \frac{m_{i, j \pm 1} + m_{i, j}}{2}$. Non zero elements of $\Sigma_P(y_j, y_{j'})$, where $j' \neq j, j \pm 1$ are neglected to ensure that A' is block tridiagonal; The algorithm to calculate G and G^n relies on the block tridiagonal form of A' . The λ appearing in eqn. (199) corresponds to the delta function in eqn. (197). λ is a diagonal matrix whose elements are given by

$$\lambda_{i,j;i,j} = \frac{4}{(x_{i+1} - x_{i-1})(y_{i+1} - y_{i-1})}. \quad (207)$$

B. Results

We will now discuss quantum mechanical aspects of transport in a two dimensional ballistic nanotransistor. We do so by comparing the current-voltage characteristics from our quantum and drift-diffusion simulations as shown in Fig. 13. The important features are a higher off-current, threshold voltage shift, smaller subthreshold slope and much higher on-current, in the quantum case.

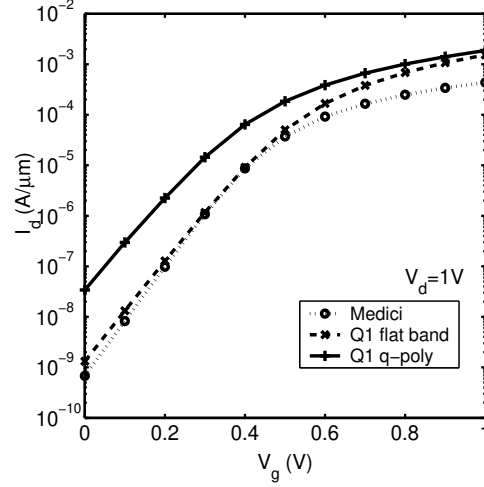


FIG. 13: Plot of drain current versus gate voltage from the quantum mechanical calculations and Medici, at $V_d = 1V$. At small gate voltages, the drain current from Medici are comparable to the 'Q1 flat band' results. The drain current from 'Q1 q-poly' is however significantly different at large gate voltages.

The change in threshold voltage results from the very different quantum mechanically calculated potential profile in the polysilicon gate. The quantum mechanical band bending is opposite to the drift-diffusion case as shown in Fig. 14. In the quantum case, the conduction band at the polysilicon-SiO₂ is lower by approximately 130 meV. The physical reason for the qualitatively different quantum potential profile arises due to the tiny quantum mechanical probability density for electron occupancy close to the barrier. As a consequence, the electronic charge density is smaller than the uniform background doping density, near the SiO₂ barrier in the polysilicon region. This causes the conduction band in the polysilicon gate to bend in a direction opposite to that computed classically.

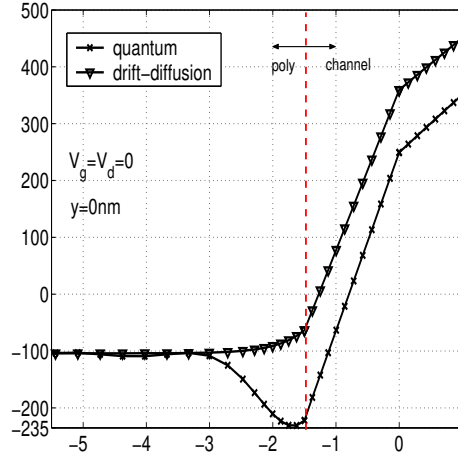


FIG. 14: Potential profile at the $y=0$ slice of MIT25, calculated using quantum and drift-diffusion methods by assuming flat band in the polysilicon gate.

The quantum mechanically calculated I_d versus V_g with and with out the quantum mechanical band bending in the gate region is shown in Fig. 15. The gate voltage shift is approximately equal to the band bending in the polysilicon gate. A shift in $I_d(V_g)$ from the flat band result by the equilibrium 1D built-in potential does a reasonable job (triangles in Fig. 15) of reproducing the results obtained by quantum mechanical treatment of the polysilicon region. This is especially true at small gate voltages and becomes progressively poorer with increase in gate voltage.

The subthreshold slope $d[\log(I_d)]/dV_g$ is smaller in the quantum case compared to the drift-diffusion case. To

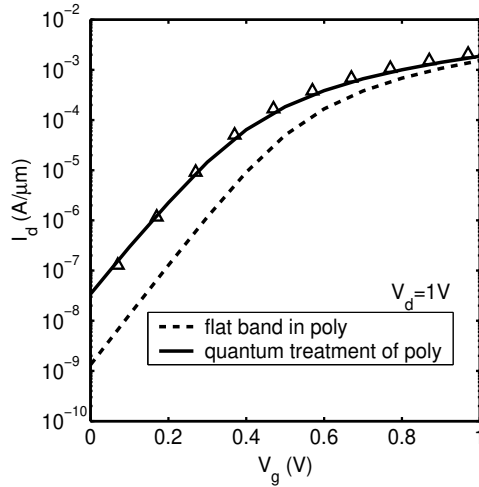


FIG. 15: Drain current versus gate voltage for $V_d = 1$ V. Quantum mechanical treatment of the polysilicon gate results in much higher current (solid line). The triangles correspond to the $I_d(V_g)$ calculated using a flat band in the polysilicon region shifted by the equilibrium built-in potential of 130 meV in the polysilicon region.

understand the reason for this, we first note that the subthreshold current resulting from the simple intuitive expression

$$I = I_{q0} e^{-\frac{E_{r1}}{kT}} \quad (208)$$

matches the quantum result quite accurately. I_{q0} is a prefactor chosen to match the current at $V_g = 0$. E_{r1} is the energy of the source injection barrier due to the lowest resonant level in the channel, which varies with gate bias. The higher resonant levels do not carry appreciable current. The difference in slope between the classical and quantum results for $I_d(V_g)$ is because of the slower variation of E_{r1} in comparison to the drift-diffusion barrier height ($E_b(\text{classical})$) as a function of V_g (Fig. 16). We also find that the decrease of E_{r1} with increase in gate voltage is slower than the barrier height determined from the quantum potential profiles. The slower variation of E_{r1} arises due to quantum confinement in the triangular well in the channel that becomes progressively narrower with increase in gate voltage (Fig. 16). This change in confinement is a non issue in the classical case.

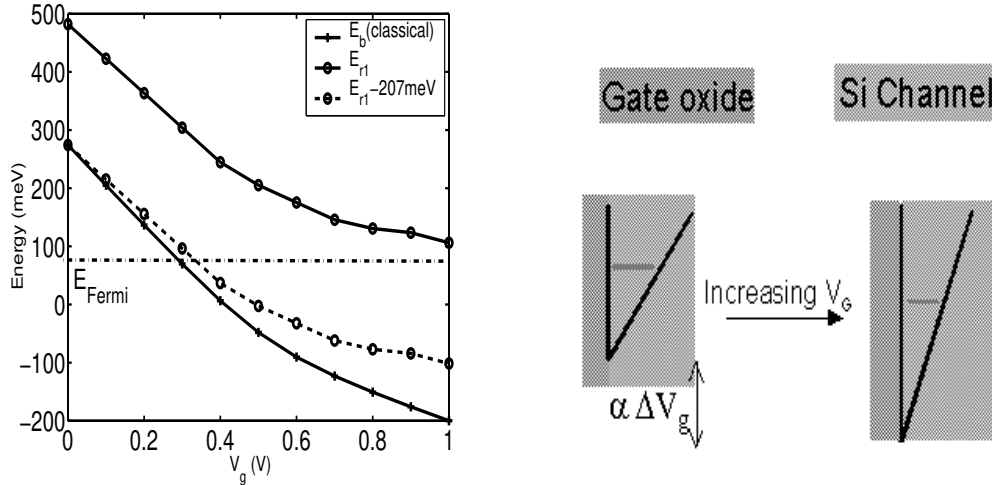


FIG. 16: *Left*: Location of the first resonant level E_{r1} versus gate voltage and the classical source injection barrier $E_b(\text{classical})$. Note that E_{r1} decreases slower than $E_b(\text{classical})$ with gate voltage due to narrowing of channel potential well. *Right*: Narrowing of the triangular well in the channel with increase in gate bias. $E_b(\text{classical})$ is the bottom of the triangular well and the resonant level is shown by the horizontal line.

We will now address the value of total transmission in a ballistic MOSFET. The transmission is related to drain

current by (eqn. (159)),

$$I_d = \frac{2e}{h} \int dE T(E) [f_S(E) - f_D(E)] , \quad (209)$$

where T is the total transmission from source to drain. f_S and f_D are the Fermi factors in the source and drain, and the factor of 2 accounts for spin. The main factors that determine the transmission probability are tunneling and scattering in the two dimensional potential profile, as an electron transits from source to drain. Traditionally, simple theories of ballistic nanotransistors have assumed that the transmission from the source to drain to be integers in the above expression for current. The quantum mechanically computed transmission versus energy is shown in Fig. 17. The transmission increases in a step-wise manner, with the integer values at plateaus equal to the number of conducting modes in the channel. The steps turn on at an energy determined by an effective 'subband dependent' source injection barrier (E_{r1}). That is, the maximum subband energy between the source and drain due to quantization perpendicular to the gate plane (x-direction of Fig. 12). The total transmission assumes integer values at an energy slightly above the maximum in 2D density of states as shown in the inset of Fig. 17. Further, the transmission steps develop over a 50 meV energy window. In the case of MIT25 the current is predominantly carried at energies where the transmission is not an integer.

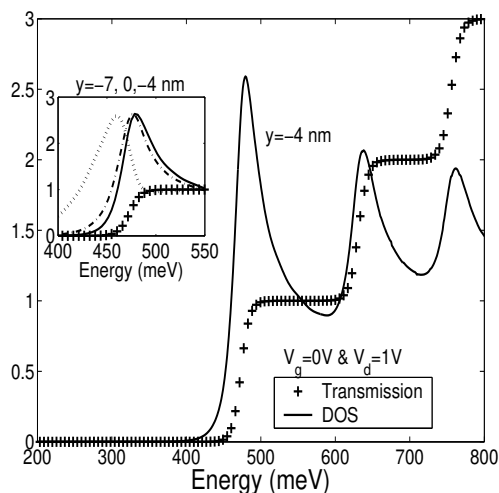


FIG. 17: Transmission (+) and density of states (solid) versus energy at a spatial location close to the source injection barrier, at $V_g = 0V$ and $V_d = 1V$. The peaks in the density of states represent the resonant levels in the channel. Inset: The density of states at three different y -locations and total transmission (+). The points $y = -7$ and 0 nm are to the left and right of the location where the source injection barrier is largest (close to $y = -4$ nm).

VIII. APPLICATION TO NANOTRANSISTORS WITH ELECTRON-PHONON SCATTERING

The channel, scattering and screening lengths become comparable in transistors with diminishing channel lengths. Carrier transport is however not fully ballistic. Realistic nanodevice modeling will involve phase-breaking scattering such that transport is between the ballistic and diffusive limits. In this regime, carriers are not thermally relaxed in the drain-end of the transistor, in contrast to long channel devices. The reflection of hot carriers from the drain-end towards the source-end, both above and below the source injection barrier should be explicitly included in models to compute the drive current. It is in this intermediate regime that the NEGF method has a distinct advantage over solving Schrodinger and Poisson equations self-consistently.

To illustrate modeling of electron-phonon scattering in nanotransistors, we consider a prototype dual gate MOSFET (DGMOSFET) with a channel length of 25 nm and channel thickness (t_{ch}) of 1.5 nm. The quantized energy levels in the channel due to quantization perpendicular to the gate (x-direction of Fig. 18) are,

$$E_n = \frac{n^2 \pi^2 \hbar^2}{2m t_{ch}^2} . \quad (210)$$

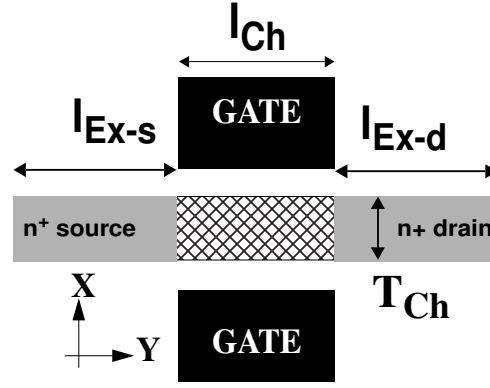


FIG. 18: Schematic of a Dual Gate MOSFET (DG MOSFET). Ex-s and Ex-d are the extension regions and the hatched region is the channel. The white region between the source / drain / channel and gate is the oxide. The device dimension normal to the page is infinite in extent.

When t_{ch} is small, the energy level separation is large and very few subbands are occupied in the highly doped extension regions. The lowest three quantized energy levels [eqn. (210)] are at 173, 691 and 891 meV above the bulk conduction band. The Fermi energy at the contact doping of $1E20 \text{ cm}^{-3}$ is 60 meV above the bulk conduction band. As a result, electrons are injected only into one subband from the source-end at the operating voltage of $V_d = V_g = 0.6V$. In this section, we discuss modeling of such MOSFETs using the mode space approach. The mode space approach consists of solving a one dimensional Schrodinger's equation for each subband. Inter subband scattering which can arise due to a change in electrostatic potential profile is neglected. Electron-phonon scattering between different subbands is included within the Born approximation.

The three dimensional effective mass Hamiltonian is the same as eqn. (193). As the z direction is infinite, the wave function can be expanded as, $\Phi(x, y, z) = e^{ik_z z} \phi(x, y)$. Schrodinger's equation is then,

$$\left[E - \frac{\hbar^2 k_z^2}{2m_z^b} - \left(-\frac{\hbar^2}{2} \frac{d}{dy} \left(\frac{1}{m_y^b} \frac{d}{dy} \right) - \frac{\hbar^2}{2} \frac{d}{dx} \left(\frac{1}{m_x^b} \frac{d}{dx} \right) + V(x, y) \right) \right] \phi(x, y) = 0. \quad (211)$$

In the first step of the mode space approach, the eigen values $[E_n(y)]$ at every cross section y along the source-drain direction is computed by solving for a subband dependent eigen value that varies with y ,

$$\left[-\frac{\hbar^2}{2m_x^b} \frac{d}{dx} \left(\frac{1}{m_x^b} \frac{d}{dx} \right) + V(x, y) \right] \Psi_n(x, y) = E_n(y) \Psi_n(x, y). \quad (212)$$

$n = \{\nu, b\}$, where ν is the quantum number due to quantization in the X-direction and $b = 1, 2$ and 3 are the valley indices.

In the second step, the Green's function equations for G , G^n and G^p are solved for each subband n :

$$\left[E - \frac{\hbar^2 k_z^2}{2m_z^n} - \left(-\frac{\hbar^2}{2} \frac{d}{dy} \left(\frac{1}{m_y^n} \frac{d}{dy} \right) + E_n(y) \right) \right] G_n(y, y', k_z, E) - \int dy_1 \Sigma_n(y, y_1, k_z, E) G_n(y_1, y', k_z, E) = \delta(y - y'), \text{ and} \quad (213)$$

$$\left[E - \frac{\hbar^2 k_z^2}{2m_z^n} - \left(-\frac{\hbar^2}{2} \frac{d}{dy} \left(\frac{1}{m_y^n} \frac{d}{dy} \right) + E_n(y) \right) \right] G_n^{(p)}(y, y', k_z, E) - \int dy_1 \Sigma_n(y, y_1, k_z, E) G_n^{(p)}(y_1, y', k_z, E) = \int dy \Sigma_n^{in(out)}(y, y_1, k_z, E) G_n^\dagger(y_1, y', k_z, E) \quad (214)$$

m_y^n and m_z^n are the effective masses of silicon in the y and z directions that give rise to subband index n . Note that in Eqs. (213) and (214), $E_n(y)$ is effectively an electrostatic potential for electrons in subband n .

We designate the Green's/correlation functions G_n^α with $\alpha \in (\text{empty}), p, n$ and, respectively, self-energies Σ_n^α with $\alpha \in (\text{empty}), out, in$. They can be written as,

$$\Sigma_n^\alpha = \Sigma_{n,C}^\alpha + \Sigma_{n,P}^\alpha, \text{ where} \quad (215)$$

$$\Sigma_{n,P}^\alpha = \Sigma_{n,el}^\alpha + \Sigma_{n,inel}^\alpha. \quad (216)$$

$\Sigma_{n,C}^\alpha$ is the self-energy due to the leads. The phonon self-energy $\Sigma_{n,P}^\alpha$ consists of two terms, $\Sigma_{n,el}^\alpha$ due to elastic and $\Sigma_{n,inel}^\alpha$ due to inelastic scattering. Scattering between the lowest three subbands due to electron-phonon interaction is included and all other inter subband scattering is neglected. The self-energy due to leads is non zero only at the first (source) and last (drain) grid points.

Assuming isotropic scattering, an equilibrium phonon bath and the self-consistent Born approximation, the self-energies due to electron-phonon scattering at grid point y_i are [Mah87],

$$\Sigma_{el,n}^\alpha(y_i, E) = \sum_{n'} D_{n,n'}^{el} \frac{\sqrt{m_z^{n'}}}{\pi \hbar \sqrt{2}} \int dE_z \frac{1}{\sqrt{E_z}} G_{n'}^\alpha(y_i, E_z, E), \quad (217)$$

$$\begin{aligned} \Sigma_{inel,n}^{in}(y_i, E) &= \sum_{n', \eta} D_{n,n'}^{i,\eta} \frac{\sqrt{m_z^{n'}}}{\pi \hbar \sqrt{2}} \int dE_z \frac{1}{\sqrt{E_z}} \\ &[n_B(\hbar\omega_\eta) G_{n'}^n(y_i, E_z, E - \hbar\omega_\eta) + (n_B(\hbar\omega_\eta) + 1) G_{n'}^n(y_i, E_z, E + \hbar\omega_\eta)] , \end{aligned} \quad (218)$$

and

$$\begin{aligned} \Sigma_{inel,n}^{out}(y_i, E) &= \sum_{n', \eta} D_{n,n'}^{i,\eta} \frac{\sqrt{m_z^{n'}}}{\pi \hbar \sqrt{2}} \int dE_z \frac{1}{\sqrt{E_z}} \\ &[n_B(\hbar\omega_\eta) G_{n'}^{p'}(y_i, E_z, E + \hbar\omega_\eta) + (n_B(\hbar\omega_\eta) + 1) G_{n'}^{p'}(y_i, E_z, E - \hbar\omega_\eta)] . \end{aligned} \quad (219)$$

Here η represents the phonon modes, and the square of the matrix elements for phonon scattering are given by,

$$D_{n,n'}^{el} = (\delta_{\nu,\nu'} + \frac{1}{2}) \delta_{b,b'} \frac{D_A^2 k T}{\rho v^2} \quad (220)$$

$$D_{n,n'}^{i,\eta} = (\delta_{\nu,\nu'} + \frac{1}{2}) \left[\delta_{b,b'} \frac{D_{g\eta}^2 \hbar}{2\rho\omega_{g\eta}} + (1 - \delta_{b,b'}) \frac{D_{f\eta}^2 \hbar}{\rho\omega_{f\eta}} \right] \quad (221)$$

The contribution to elastic scattering is only from acoustic phonon scattering. The values of the deformation potential, D_A , $D_{g\eta}$ and $D_{f\eta}$, and phonon frequencies $\omega_{g\eta}$ and $\omega_{f\eta}$ are taken from [Lun00]. ρ is the mass density, k is the Boltzmann constant, T is the temperature and v is the velocity of sound. b and b' are indices representing the valley. The following scattering processes are included: acoustic phonon scattering in the elastic approximation and g-type intervalley scattering with phonon energies of 12, 19 and 62 meV. The imaginary part of the electron-phonon self-energy which is responsible for scattering induced broadening of energy levels and energetic redistribution of carriers are included but the real part is set to zero.

In the numerical solution, N uniformly spaced grid points in the Y -direction with the grid spacing equal to Δy are considered. The discretized form of Eqs. (213) and (214) are then:

$$A_{i,i} G_n(y_i, y'_i, k_z, E) + A_{i,i+1} G_n(y_{i+1}, y'_i, k_z, E) + A_{i,i-1} G_n(y_{i-1}, y'_i, k_z, E) = \frac{\delta_{i,i'}}{\Delta y}, \quad \text{and} \quad (222)$$

$$\begin{aligned} A_{i,i} G_n^\alpha(y_i, y'_i, k_z, E) + A_{i,i+1} G_n^\alpha(y_{i+1}, y'_i, k_z, E) + A_{i,i-1} G_n^\alpha(y_{i-1}, y'_i, k_z, E) = \\ \Sigma_n^\alpha(y_i, E) G_n^\dagger(y_i, y'_i, k_z, E), \end{aligned} \quad (223)$$

where,

$$A_{i,i} = E - \frac{\hbar^2 k_z^2}{2m_z^n} - \frac{\hbar^2}{m_y^n \Delta y^2} - E_n(y_i) - \Sigma_n(y_i, k_z, E) \quad \text{and} \quad (224)$$

$$A_{i\pm 1,i} = + \frac{\hbar^2}{2m_z^n \Delta y^2} \quad (225)$$

The contact self-energies are:

$$\Sigma_{n,C}(y_1, k_z, E) = \left(\frac{\hbar^2}{2m_z^n \Delta y^2}\right)^2 g_s(k_z, E) \quad (226)$$

$$\Sigma_{n,C}(y_N, k_z, E) = \left(\frac{\hbar^2}{2m_z^n \Delta y^2}\right)^2 g_d(k_z, E) \quad (227)$$

$$\Sigma_{n,C}^{in}(y_1, k_z, E) = -2\text{Im}(\Sigma_{n,C}(y_1, k_z, E))f_s(E) \quad (228)$$

$$\Sigma_{n,C}^{in}(y_N, k_z, E) = -2\text{Im}(\Sigma_{n,C}(y_N, k_z, E))f_d(E) \quad (229)$$

$$\Sigma_{n,C}^{out}(y_1, k_z, E) = -2\text{Im}(\Sigma_{n,C}(y_1, k_z, E))[1 - f_s(E)] \quad (230)$$

$$\Sigma_{n,C}^{out}(y_N, k_z, E) = -2\text{Im}(\Sigma_{n,C}(y_N, k_z, E))[1 - f_d(E)] , \quad (231)$$

where y_1 and y_N are the left (source-end) and right (drain-end) most grid points respectively, $g_s(k_z, E)$ and $g_d(k_z, E)$ are the surface Green's functions of the source and drain leads respectively, and f_s and f_d are the Fermi functions in the source and drain contacts respectively.

The electron and current densities per energy given by Eqs. (128) and (149) can be simplified to

$$n_n(y_i, k_z, E) = G_n^n(y_i, y_i, k_z, E) \quad (232)$$

$$J_n(y_i, k_z, E) = \frac{ie}{\hbar} \sum_n \frac{\hbar^2}{2m_y^n \Delta y^2} [G_n^n(y_i, y_{i+1}, k_z, E) - G_n^n(y_{i+1}, y_i, k_z, E)] . \quad (233)$$

The total electron and current densities at grid point y_i are given by,

$$n(y_i) = 4 \sum_n \frac{\sqrt{m_z^{n'}}}{\pi \hbar \sqrt{2}} \int \frac{dE}{2\pi} \int dE_z \frac{1}{\sqrt{E_z}} n_n(y_i, E_z, E) \quad (234)$$

$$J(y_i) = 4 \sum_n \frac{\sqrt{m_z^{n'}}}{\pi \hbar \sqrt{2}} \int \frac{dE}{2\pi} \int dE_z \frac{1}{\sqrt{E_z}} J_n(y_i, E_z, E) , \quad (235)$$

where the prefactor of 4 in the above two equations account for two fold spin and valley degeneracies. The non equilibrium electron and current densities are calculated in both the channel and extension regions using the algorithm for G^n presented in section C 2.

In solving the the Green's function and Poisson's equation, the applied bias corresponds to a difference in the Fermi levels used in the source and drain regions. The electrostatic potential at the left and right most grid points of the source and drain extension regions are calculated self consistently using the floating boundary condition that $dV(y)/dy = 0$. Poisson's equation is solved in two dimensions and the electron density is computed from Eqs. (212) and (232) using,

$$n(x_i, y_i, k_z, E) = n_n(y_i, k_z, E) |\Psi_n(x_i, y_i)|^2 . \quad (236)$$

When does the mode-space approach fail? Ref. [Ven03] has extensively analysed the regime of validity of the mode space approach. The mode space approach is valid when the wave function $\Psi_n(x, y)$ at various y cross sections in eqn. (212) satisfies $\frac{\Psi_n(x, y)}{dy} \sim 0$. That is the shape of the wave function at each cross section should not change significantly along the transport direction, which means that intersubband scattering due to changes in potential profile is absent. This approximation seems to be valid until a channel thickness of 5 nm for silicon.

A. Results

Using the equations presented in the previous section, we show results illustrating the role of scattering along the channel length of a nanotransistor. First, we show that in devices where the scattering length is comparable to channel length, the nanotransistor drive current is affected by scattering at all points in the channel. Second, we show that when hot electrons enter the drain extension region of a nanotransistor, the drain extension region cannot be modeled as a series resistance. Instead, the drain extension should be included as part of the non equilibrium simulation region.

To illustrate the role of scattering along the channel, we calculate the drain current as a function of the *right boundary of scattering* ($Y_{R-Scatt}$) [Svi03]. Scattering is included only from the source end of the channel (-5 nm) to $Y_{R-Scatt}$ by setting the deformation potential in Eqs. (220) and (221) to zero to the right of $Y_{R-Scatt}$. The scattering

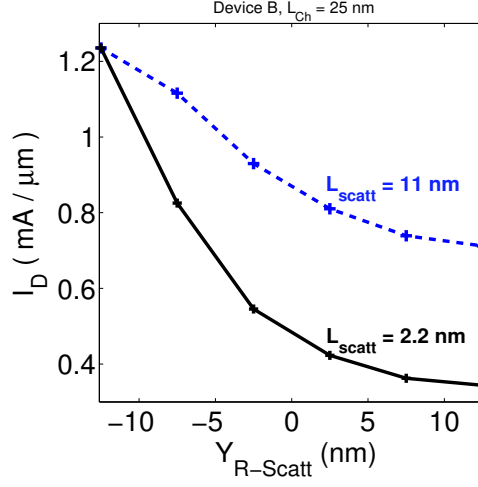


FIG. 19: Drain current versus $Y_{R-Scatt}$ for two different scattering lengths. The channel length is 25 nm.

lengths are decreased by a factor α by modifying the deformation potential in Eqs. (220) and (221) by an overall multiplicative factor of $\sqrt{\alpha}$.

The device considered has a channel length of 25 nm, body thickness of 1.5 nm, oxide thickness of 1.5 nm, doping of $1 \text{ E}+20 \text{ cm}^{-3}$ in the source and drain extension regions and an intrinsic channel. The scattering length due to electron-phonon interaction is 11 nm. We see from Fig. 19 that scattering in the right half of the channel (0 to 12.5 nm) is important and that the drive current degradation due to scattering in the right half of the channel is 30%. To understand the large reduction in drain current due to scattering in the right half of the channel, we plot the current density as a function of energy at various cross sections, $J(Y, E)$. $J(Y, E)$ shows the energetic redistribution of carriers along the channel. When the channel length is comparable to the scattering length, $J(Y, E)$ in the right half of the channel is peaked in energy above the source injection barrier as shown in Fig. 20 (a). Scattering causes reflection of these energetic electrons toward the source. These reflected electrons lead to an increase in the channel electron density (classical MOSFET electrostatics). As the charge in the channel should be approximately $C_{ox}(V_G - V_S)$, the source injection barrier floats to a higher energy to compensate for the reflected electrons. The increase in source injection barrier and reflection leads to the decrease in drain current [Lun97].

To gain further insight into the role of carrier relaxation, we now discuss the case when the scattering length is 2.2 nm, which is five times smaller than in the previous discussion. We see from Fig. 19 that scattering in the right half of the channel now decreases the drive current by a smaller amount of 15%, when compared to the case with $L_{scatt} = 11$ nm. As the channel length of 25 nm is much larger than 2.2 nm, multiple scattering events now lead to an energy distribution of current that is peaked well below the source injection barrier in the right half of the channel as shown in Fig. 20 (b). The first moment of energy with respect to the current distribution function, which is defined as the ratio of $\int dE E J(Y, E)$ and total current is also shown in Fig. 20. When the scattering length is much smaller than the channel length, the carriers relax classically such that the first moment ($\int dE E J(Y, E)$) closely tracks the potential profile as seen in Fig. 20 (b). Thermalized carriers that are reflected in the right half of the channel can no longer reach the source injection barrier due to the large barrier to the left, and so contribute less significantly to the charge density. Thus, explaining the diminished influence of scattering in the right half of the channel relative to the left half of the channel.

To further demonstrate the use of NEGF simulations, we study the role of assuming that the extension regions can be modeled as a classical series resistance. Within the classical series resistance picture the current with scattering (I_D^{scatt}) can be related to the current without scattering ($I_D^{noscatt}$) by [Tau98],

$$I_D^{scatt}(V_D) \sim I_D^{noscatt}(V_D - \delta V_D), \quad (237)$$

where we have assumed that the source extension region and device do not experience scattering. The potential drop in the drain region within the classical series resistance picture is $\delta V_D = I_D^{scatt}(V_D) R_D$. In Fig. 21, the values of the drain current in the ballistic limit, using the classical series resistance picture and with the NEGF method are marked. Clearly, the series resistance picture underestimates the detrimental nature of scattering in the drain end. The physics of the large reduction in drain current was discussed in the context of Fig. 20: When scattering in the channel does not effectively thermalize carriers, the current distribution is peaked at energies above the source

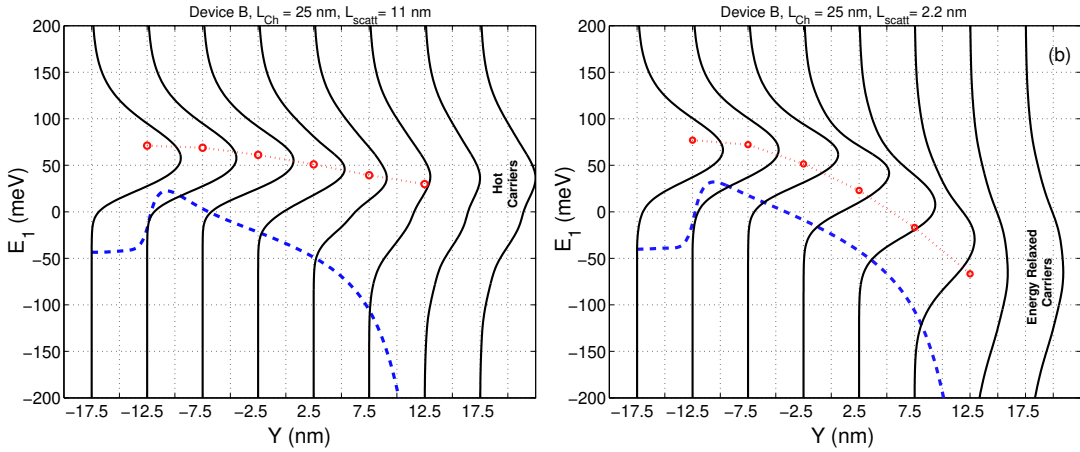


FIG. 20: Solid lines represent $J(Y, E)$ for Y equal to $-17.5, -12.5, -7.5, -2.5, 2.5, 7.5, 12.5, 17.5$ nm respectively, when scattering is included every where in the channel. The dashed lines are the first resonant level (E_1) along the channel. The dotted lines represent the first moment of energy with respect to the current distribution function, $\int dE E J(Y, E)$. (a) and (b) correspond to $L_{scatt} = 11$ and 2.2 nm respectively.

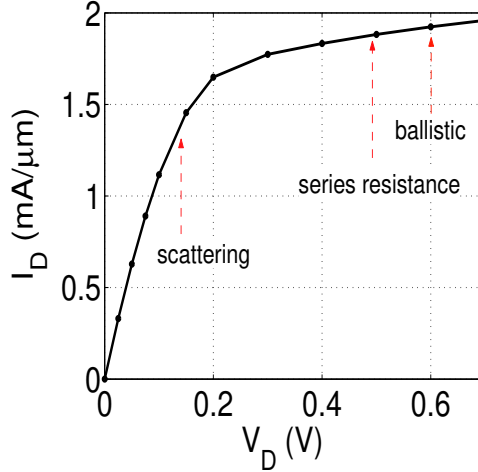


FIG. 21: Ballistic $I_D(V_D)$ with the drive currents obtained in the ballistic limit, with the series resistance picture and NEGF calculations marked.

injection barrier, upon carriers exiting the channel. Scattering in the drain extension region then causes reflection of electrons toward the source-end. As a result, the source injection increases so as to keep the electron density in the channel approximately at $C_{ox}(V_G - V_S)$. The drain current decreases dramatically as a result of the increase in source injection barrier height.

IX. DISCUSSION AND SUMMARY

Our objectives in this chapter has been to: (i) review the underlying assumptions of the traditional, semiclassical treatment of carrier transport in semiconductor devices, (ii) describe how the semiclassical approach can be applied to ballistic transport, (iii) discuss the Landauer-Buttiker approach to quantum transport in the phase coherent limit, (iv) introduce important elements of the non-equilibrium Green's function approach using Schrodinger's equation as a starting point and (v) finally demonstrate the application of the NEGF method to the MOSFET in the ballistic limit and with electron-phonon scattering.

It is appropriate to make a few comments about the computational burden of the various transport models. One

reason that device engineers continue to use drift-diffusion simulations rather than the more rigorous Monte Carlo simulations is the enormous difference in computational burden. For semiclassical transport, the fundamental quantity is the carrier distribution function, $f(\vec{r}, \vec{k}, t)$. To find $f(\vec{r}, \vec{k})$, we must solve the BTE, which is a six-dimensional equation. The difficulty of solving this six-dimensional equation is one reason that engineers continue to rely on simplified models. For quantum transport, we can take the Green's function $G^n(\vec{r}, \vec{r}', E)$ as the fundamental quantity. The Green's function is a correlation function that describes the phase relationship between the wavefunction at \vec{r} and \vec{r}' for an electron injected at energy E . The quantum transport problem is seven dimensional, which makes it much harder than the semiclassical problem. We can think of \vec{r} and \vec{r}' as analogous to \vec{r} and \vec{k} in the semiclassical approach, but there is no E in the semiclassical approach. The reason is that for a bulk semiconductor or in a device in which the potential changes slowly, there is a relation between E and \vec{k} , as determined by the semiconductor bandstructure $E(\vec{k})$. When the potential varies rapidly, however, there is no $E(\vec{k})$, and energy becomes a separate dimension. Analysis of electronic devices by quantum simulation is however becoming practical because device dimensions are shrinking, which reduces the size of the problem. Quantum simulations are also essential to accurately model devices whose dimensions are comparable to the phase breaking length, and rely on tunneling and wave interference for operation. The resonant tunneling diode is the most successful example in this category.

X. ACKNOWLEDGEMENTS

MPA is grateful to T. R. Govindan and Alexei Svizhenko for collaboration and discussions over the last five years. MPA and DEN would also like to thank Supriyo Datta for many useful discussions.

APPENDIX A: DERIVATION OF EQN. (60)

Eq. (59) can be expanded as,

$$G_{LD} = -A'_{LL}{}^{-1}A'_{LD}G_{DD} \quad (\text{A1})$$

$$G_{RD} = -A'_{RR}{}^{-1}A'_{RD}G_{DD} \quad (\text{A2})$$

$$A'_{DL}G_{LD} + A'_{DD}G_{DD} + A'_{DR}G_{RD} = I. \quad (\text{A3})$$

Substituting Eqs. (A1) and (A2) in eqn. (A3), we have,

$$[A'_{DD} - A'_{DL}A'_{LL}{}^{-1}A'_{LD} - A'_{DR}A'_{RR}{}^{-1}A'_{RD}]G_{DD} = I. \quad (\text{A4})$$

Noting the sparsity of A'_{LD} and A'_{RD} , it follows that only the **surface Green's functions** of the Left and Right leads,

$$g_{L_{-1,-1}} = A'_{LL_{1,1}}{}^{-1} \quad \text{and} \quad g_{R_{n+1,n+1}} = A'_{RR_{1,1}}{}^{-1} \quad (\text{A5})$$

are required in eqn. (A4). Then, we can rewrite eqn. (A4) in terms of lead self-energies as,

$$AG_{DD} = [EI - H_D - \Sigma_{lead}]G_{DD} = I, \quad (\text{A6})$$

where Σ_{lead} has been defined in eqn. (52) and (53). The reader can verify that $g_{L_{-1,-1}} = e^{+ik_l a} t_l^{-1}$ and $g_{R_{n+1,n+1}} = e^{+ik_r a} t_r^{-1}$.

APPENDIX B: DYSON'S EQUATION FOR LAYERED STRUCTURES

(**Note:** Matrix A of this section is equivalent to Matrix A_{DD} of section VI)

Partition the device layers into two regions Z and Z' as shown in Fig. 22. Dyson's equation is a very useful method that relates the Green's function of the full system $Z + Z'$ in terms of the subsystems Z , Z' and the coupling between Z and Z' . We will see below that from a computational point of view, Dyson's equation provides us with a systematic framework to calculate the diagonal blocks of G and G^n without full inversion of the A matrix. The reader should note that Dyson's equation has a significantly more general validity than implied in our application here [Mah90].

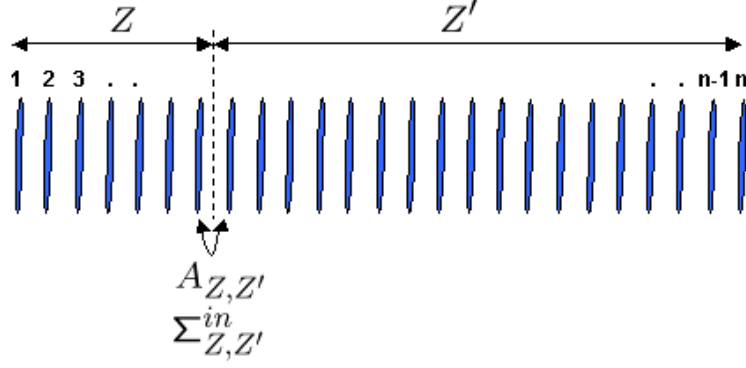


FIG. 22: Scheme of device for application of Dyson's equation by splitting the device in two parts.

1. Dyson's equation for G

The Green's function equation over the device layers [eqn. (122)],

$$AG = I \quad (\text{B1})$$

can be written as,

$$\begin{pmatrix} A_{Z,Z} & A_{Z,Z'} \\ A_{Z',Z} & A_{Z',Z'} \end{pmatrix} \begin{pmatrix} G_{Z,Z} & G_{Z,Z'} \\ G_{Z',Z} & G_{Z',Z'} \end{pmatrix} = \begin{pmatrix} I & O \\ O & I \end{pmatrix}. \quad (\text{B2})$$

The solution of eqn. (B1) is,

$$G = G^0 + G^0 U G \quad (\text{B3})$$

$$= G^0 + G U G^0, \quad (\text{B4})$$

where,

$$G = \begin{pmatrix} G_{Z,Z} & G_{Z,Z'} \\ G_{Z',Z} & G_{Z',Z'} \end{pmatrix}, G^0 = \begin{pmatrix} G_{Z,Z}^0 & O \\ O & G_{Z',Z'}^0 \end{pmatrix} = \begin{pmatrix} A_{Z,Z}^{-1} & O \\ O & A_{Z',Z'}^{-1} \end{pmatrix} \text{ and } U = \begin{pmatrix} O & -A_{Z,Z'} \\ -A_{Z',Z} & O \end{pmatrix}. \quad (\text{B5})$$

The Hermitean conjugate Green's function (G^\dagger) is by definition related to G by

$$G^\dagger = G^{\dagger 0} + G^{\dagger 0} U^\dagger G^\dagger \quad (\text{B6})$$

$$= G^{\dagger 0} + G^\dagger U^\dagger G^{\dagger 0}. \quad (\text{B7})$$

Eq. (B3) is Dyson's equation for the Green's function.

2. Dyson's equation for G^n

The electron correlation function equation over the device layers [eqn. (131)],

$$AG^n = \Sigma^{in} G^\dagger \quad (\text{B8})$$

can be written as,

$$\begin{pmatrix} A_{Z,Z} & A_{Z,Z'} \\ A_{Z',Z} & A_{Z',Z'} \end{pmatrix} \begin{pmatrix} G_{Z,Z}^n & G_{Z,Z'}^n \\ G_{Z',Z}^n & G_{Z',Z'}^n \end{pmatrix} = \begin{pmatrix} \Sigma_{Z,Z}^{in} & \Sigma_{Z,Z'}^{in} \\ \Sigma_{Z',Z}^{in} & \Sigma_{Z',Z'}^{in} \end{pmatrix} \begin{pmatrix} G_{Z,Z}^\dagger & G_{Z,Z'}^\dagger \\ G_{Z',Z}^\dagger & G_{Z',Z'}^\dagger \end{pmatrix}. \quad (\text{B9})$$

The solution of eqn. (B8) is,

$$G^n = G^0 U G^n + G^0 \Sigma^{in} G^\dagger, \quad (\text{B10})$$

where G^0 and U have been defined in Eqs. (B5). Functions G^n and G^\dagger are readily defined by eqns. (B8) and (B7), respectively. Using $G^\dagger = G^{\dagger 0} + G^{\dagger 0}U^\dagger G^\dagger$, eqn. (B10) can be written as

$$G^n = G^{m0} + G^{m0}U^\dagger G^\dagger + G^0UG^n \quad (\text{B11})$$

$$= G^{m0} + GUG^{m0} + G^nU^\dagger G^{\dagger 0}, \quad (\text{B12})$$

$$\text{where } G^{m0} = G^0\Sigma^{in}G^{\dagger 0}. \quad (\text{B13})$$

APPENDIX C: ALGORITHM TO CALCULATE G AND G^n

(**Note:** Matrix A of this section is equivalent to Matrix A_{DD} of section VI)

Why algorithm: A typical simulation of a nanoelectronic device consists of solving Poisson's equation self-consistently with the Green's function equations. The input to Poisson's equation is the charge density, which is obtained via integrating over energies the elements, $G_{q,q}^n(E)$, from the main diagonal of the electron correlation function. The index q here runs over the layers of the device. In order to calculate the current density one requires the elements, $G_{q,q+1}^n(E)$, from the diagonals adjacent to the main diagonal. That is, we *do not* require the entire G^n matrix in most situations. Same goes for the hole correlation function G^p and the Green's function G .

Provided that N_x is the dimension of the Hamiltonian of each layer and N_y is the total number of layers, the size of the matrix A equals $N_x N_y$. The operation count for the full matrix inversion $G = A^{-1}$ is proportional to $(N_x N_y)^3$. The computational cost of obtaining the diagonal elements of the G^n matrix at each energy is approximately $N_x^3 N_y^3$ operations if $G^n = G\Sigma^{in}G^\dagger$ is used. Therefore it is highly desirable to find less expensive algorithms that avoid full inversion of matrix A and take advantage of the fact the diagonal elements of Green's functions. Another reason to prefer such algorithms is the memory storage. If one had had to retain the whole matrix G in the memory, it might had required using the RAM or the hard drive instead of on-chip cache. That would have significantly slowed down the calculations.

One such algorithm which is valid for the block tridiagonal form of matrix A is presented in this section. The operation count of this algorithm scales approximately as $N_x^3 N_y$. The dependence on N_x^3 arises because matrices of dimension of the sub Hamiltonian of layers should be inverted, and the dependence on N_y corresponds to one such inversion for each of the N_y layers.

The algorithm consists of two steps. In the first step, the diagonal blocks of the left connected and full Green's function are evaluated (section C1). In the second step, these results are used to evaluate the diagonal blocks of the less-than Green's function (section C2).

1. Recursive algorithm for G

(i) Left-connected Green's function (Fig. 23):

The left-connected (superscript L) Green's function g^{Lq} is defined by the first q blocks of eqn. (122) by

$$A_{1:q,1:q} g^{Lq} = I_{q,q}. \quad (\text{C1})$$

where we introduce a shorthand $I_{q,q} = I_{1:q,1:q}$. The matrix g^{Lq+1} is defined in a manner identical to g^{Lq} except that the left-connected system is comprised of the first $q+1$ blocks of eqn. (122). In terms of eqn. (B2), the equation governing g^{Lq+1} can be expressed via the solution g^{Lq} by setting $Z = 1 : q$ and $Z' = q + 1$. Using Dyson's equation [eqn. (B3)], we obtain

$$g_{q+1,q+1}^{Lq+1} = (A_{q+1,q+1} - A_{q+1,q}g_{q,q}^{Lq}A_{q,q+1})^{-1}. \quad (\text{C2})$$

Note that the last element of this progression g^{LN} is equal to the fully connected Green's function G , which is the solution to eqn. (122).

(ii) Full Green's function in terms of the left-connected Green's function:

Consider the special case of eqn. (B2) in which $A_{Z,Z} = A_{1:q,1:q}$, $A_{Z',Z'} = A_{q+1:N,q+1:N}$ and $A_{Z,Z'} = A_{1:q,q+1:N}$. Noting that the only nonzero element of $A_{1:q,q+1:N}$ is $A_{q,q+1}$ and using eqn. (B3), we obtain

$$G_{q,q} = g_{q,q}^{Lq} + g_{q,q}^{Lq} (A_{q,q+1}G_{q+1,q+1}A_{q+1,q}) g_{q,q}^{Lq} \quad (\text{C3})$$

$$= g_{q,q}^{Lq} - g_{q,q}^{Lq} A_{q,q+1} G_{q+1,q}. \quad (\text{C4})$$

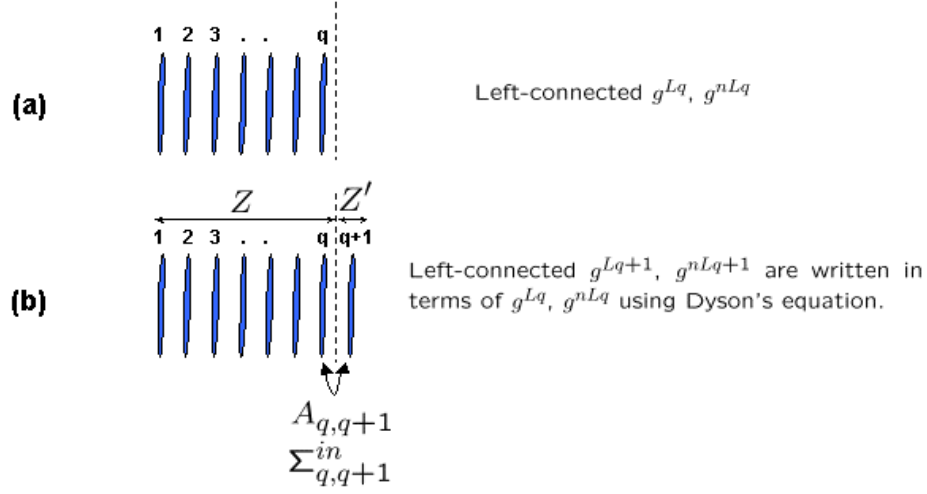


FIG. 23: Illustration for the relation between the left-connected Green's functions for adjacent layers.

The equations for the adjacent diagonals are obtained similarly

$$G_{q+1,q} = -G_{q+1,q+1}A_{q+1,q}g_{q,q}^{Lq}, \quad (\text{C5})$$

$$G_{q,q+1} = -g_{q,q}^{Lq}A_{q,q+1}G_{q+1,q+1}. \quad (\text{C6})$$

Both $G_{q,q}$ and $G_{q+1,q}$ are used in the algorithm for electron density, and so storing both sets of matrices is necessary. Making use of the above equations, the algorithm to obtain the three diagonals of G is

1. $g_{11}^{L1} = A_{11}^{-1}$.
2. For $q = 1, 2, \dots, N-1$, compute eqn. (C2).
3. For $q = 1, 2, \dots, N$, compute $(g_{qq}^{Lq})^\dagger$.
4. $G_{N,N} = g_{q,q}^{Lq}$.
5. For $q = N-1, N-2, \dots, 1$, compute eqns. (C5), (C6) and (C4) (in this order).
6. For $q = 1, 2, \dots, N$, compute $(G_{q,q+1})^\dagger$ and $(G_{q+1,q})^\dagger$.

2. Recursive algorithm for G^n

(i) Left-connected G^n (Fig. 23):

The function g^{nLq} is the counterpart of g^{Lq} , and is defined by the first q blocks of eqn. (131):

$$A_{1:q,1:q} g^{nLq} = \sum_{1:q,1:q}^{in} g_{1:q,1:q}^{\dagger Lq}. \quad (\text{C7})$$

g^{nLq+1} is defined in a manner identical to g^{nLq} except that the left-connected system is comprised of the first $q+1$ blocks of eqn. (131).

The equation governing g^{nLq+1} follows from eqn. (B9) by setting $Z = 1 : q$ and $Z' = q+1$. Using the Dyson's equations for G [eqn. (B3)] and G^n [eqn. (B11)], $g_{q+1,q+1}^{nLq+1}$ is recursively obtained as

$$g_{q+1,q+1}^{nLq+1} = g_{q+1,q+1}^{Lq+1} [\sum_{q+1,q+1}^{in} + \sigma_{q+1}^{in}] g_{q+1,q+1}^{Lq+1\dagger}, \quad (\text{C8})$$

where $\sigma_{q+1}^{in} = A_{q+1,q} g_{q,q}^{nLq} A_{q,q+1}^\dagger$. Eqn. (C8) has the physical meaning that $g_{q+1,q+1}^{nLq+1}$ has contributions due to an effective self-energy due to the left-connected structure that ends at q , which is represented by σ_{q+1}^{in} and the diagonal self-energy component at grid point $q+1$ (\sum_{DD}^{in} of eqn. (131)).


```

Al_cr = conj(Au);
Ad_cr = conj(Ad); % Hermitean conjugate of the coefficient matrix
Au_cr = conj(Al);
grL = zeros(1,Np); % initialize left-connected function
ginL = zeros(1,Np); % initialize left-connected in-scattering function
gipL = zeros(1,Np); % initialize left-connected out-scattering function
Grl = zeros(1,Np-1);
Grd = zeros(1,Np); % initialize the Green's function
Gru = zeros(1,Np-1);
Gnl = zeros(1,Np-1);
Gnd = zeros(1,Np); % initialize the electron coherence function
Gnu = zeros(1,Np-1);
Gpl = zeros(1,Np-1);
Gpd = zeros(1,Np); % initialize the hole coherence function
Gpu = zeros(1,Np-1);
grL(1)=1/Ad(1); % step 1
for q=2:Np % obtain the left-connected function
    grL(q)=1/(Ad(q)-Al(q-1)*grL(q-1)*Au(q-1));
end
gaL = conj(grL); % advanced left-connected function
Grd(Np)=grL(Np); % step 2
for q=(Np-1):-1:1
    Grl(q)=-Grd(q+1)*Al(q)*grL(q); % obtain the sub-diagonal of the Green's function
    Gru(q)=-grL(q)*Au(q)*Grd(q+1); % obtain the super-diagonal of the Green's function
    Grd(q)=grL(q)-grL(q)*Au(q)*Grl(q); % obtain the diagonal of the Green's function
end
Gal = conj(Gru);
Gad = conj(Grd); % advanced Green's function
Gau = conj(Gal);
ginL(1)=grL(1)*Sigin(1)*gaL(1); % step 3
for q=2:Np
    sla2 = Al(q-1)*ginL(q-1)*Au_cr(q-1);
    prom = Sigin(q) + sla2;
    ginL(q)=grL(q)*prom*gaL(q); % left-connected in-scattering function
end
Gnd(Np)=ginL(Np); % step 4
Gnd = real(Gnd);
for q=(Np-1):-1:1
    Gnl(q) = - Grd(q+1)*Al(q)*ginL(q) - Gnd(q+1)*Al_cr(q)*gaL(q);
    % obtain the lower diagonal of the electron Green's function
    Gnd(q) = ginL(q) + grL(q)*Au(q)*Gnd(q+1)*Al_cr(q)*gaL(q) ...
    - ( ginL(q)*Au_cr(q)*Gal(q) + Gru(q)*Al(q)*ginL(q) );
end
Gnu = conj(Gnl); % upper diagonal of the electron function
switch flag_Gp
    case 'yes'
gipL(1)=grL(1)*Sigout(1)*gaL(1); % step 3
for q=2:Np
    sla2 = Al(q-1)*gipL(q-1)*Au_cr(q-1);
    prom = Sigout(q) + sla2;
    gipL(q)=grL(q)*prom*gaL(q); % left-connected in-scattering function
end
Gpd(Np)=gipL(Np); % step 4
Gpd = real(Gpd);
for q=(Np-1):-1:1
    Gpl(q) = - Grd(q+1)*Al(q)*gipL(q) - Gnd(q+1)*Al_cr(q)*gaL(q);
    % obtain the lower diagonal of the hole Green's function
    Gpd(q) = gipL(q) + grL(q)*Au(q)*Gpd(q+1)*Al_cr(q)*gaL(q) ...

```

```

- ( gipL(q)*Au_cr(q)*Gal(q) + Gru(q)*Al(q)*gipL(q) );
end
Gpu = conj(Gpl); % upper diagonal of the hole function
case 'no'
Gpl = i*(Grl-Gal) - Gnl;
Gpd = real(i*(Grd-Gad) - Gnd); % hole Green's function
Gpu = i*(Gru-Gau) - Gnu;
end
jnzer = find(Gnd<0);
Gnd(jnzer) = 0;
jpzer = find(Gpd<0);
Gpd(jpzer) = 0;
%%%%%%%%%%%%%%%%%%%%%%%%%%%%%%%%%%%%%%%%%%%%%%%%%%%%%%%%%%%%%%%%%%%%%%%%

```

APPENDIX E: REFERENCES

-
- [But92] M. Buttiker, "Scattering theory of current and intensity noise correlations in conductors and wave guides", Phys. Rev. B, v. 46, p. 12485 (1992).
- [Dat96] S. Datta, *Electronic Conduction in Mesoscopic Systems*, Cambridge University Press, Cambridge, UK, 1996.
- [Jac89] C. Jacoboni, P. Lugli, *The Monte Carlo Method for Semiconductor Device Simulation*, Springer-Verlag, New York, 1989.
- [Lun00] M. S. Lundstrom, *Fundamentals of Carrier Transport*, 2nd ed., Cambridge University Press, Cambridge, UK, 2000.
- [Lun97] M. S. Lundstrom, "Elementary scattering theory of the MOSFET", IEEE Electron. Device Lett., v. 18, p. 361 (1997).
- [Mah87] G. D. Mahan, "Quantum transport equation for electric and magnetic fields", Physics Reports, v. 145, p. 251 (1987).
- [Mah90] G. D. Mahan, *Many Particle Physics*, Plenum, 1990.
- [Mei90] Y. Meir and N.S. Wingreen, "Landauer Formula for the Current through an Interacting Electron Region", Phys. Rev. Lett., v. 68, p. 2512 (1992).
- [Pie87] R. F. Pierret, *Advanced Semiconductor Fundamentals*, Addison-Wesley, Reading, Massachusetts, 1987.
- [Ren03] Z. Ren, R. Venugopal, S. Goasguen, S. Datta, and M. S. Lundstrom "nanoMOS 2.5: A Two -Dimensional Simulator for Quantum Transport in Double-Gate MOSFETs," IEEE Trans. Electron. Dev., and IEEE Trans. Nanotechnology, joint special issue on Nanoelectronics, v. 50, p. 1914 (2003).
- [Rhe02] J.-H. Rhew, Z. Ren, and M. Lundstrom, "A Numerical Study of Ballistic Transport in a Nanoscale MOSFET," Solid-State Electronics, v. 46, p. 1899 (2002).
- [Sho50] W. Shockley, *Electrons and Holes in Semiconductors*, von Nostrand, 1950.
- [Svi02] A. Svizhenko, M. P. Anantram, T. R. Govindan, B. Biegel, and R. Venugopal, "Two Dimensional Quantum Mechanical Modeling of Nanotransistors", J. Appl. Phys., v. 91, p. 2343 (2002).
- [Svi03] A. Svizhenko and M. P. Anantram, "Role of Scattering in Nanotransistors", IEEE Trans. Elec. Dev., v. 50, p. 1459 (2003).
- [Tau98] Y. Taur and T. H. Ning, *Fundamentals of Modern VLSI Devices*, Cambridge University Press, Cambridge, UK, 1998.
- [Ven03] R. Venugopal, Z. Ren, S. Datta, M. S. Lundstrom and D. Jovanovic, "Simulating quantum transport in nanoscale transistors: Real versus mode-space approaches", J. Appl. Phys., v. 92, p. 3730 (2003).